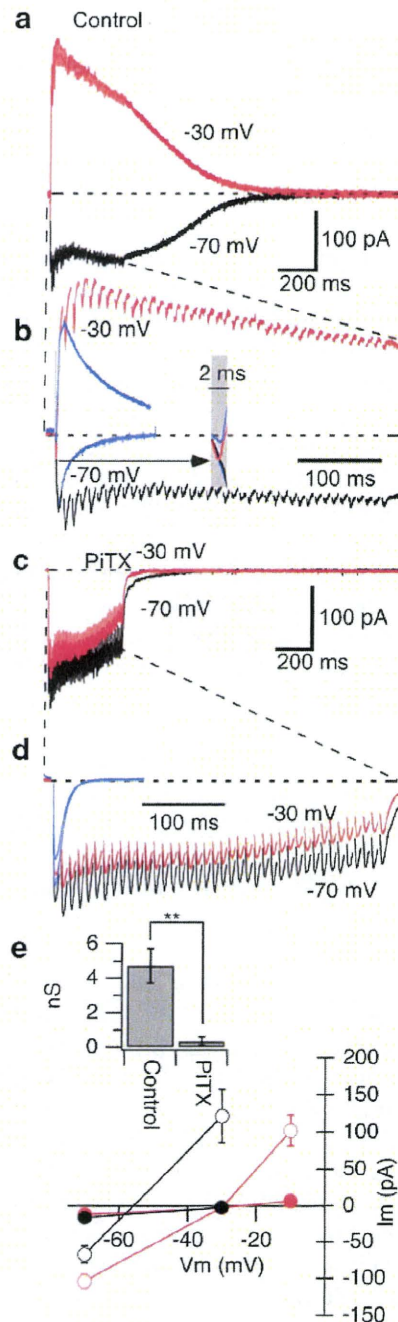


**Fig. 3** Incremental inhibition of EPSC components with a depolarized holding potential (a, b) and in the presence of the GABA<sub>A</sub> receptor antagonist PiTX (c, d); recorded with Cs-MeSO<sub>3</sub>-based, low Cl<sup>-</sup> internal pipette solution. a, b Representative membrane current response to tetanic stimulation superimposed on responses to a single stimulation (blue traces). Holding potential was -70 mV (black traces) and -30 mV (red traces) for each case. Time expanded traces of the first part (gray) are superimposed in b middle. c, d Representative membrane current responses in the presence of PiTX. e Current-voltage relationships of the long-lasting tail components measured at 50 ms from the cessation of stimulus train in the control (open circle) and PiTX (close circle) condition recorded with low Cl<sup>-</sup> pipette internal solution ( $E_{Cl} = -73$  mV, black symbols) and higher Cl<sup>-</sup> pipette internal solution ( $E_{Cl} = -29$  mV, red symbols). Conductance calculated from the current-voltage relationships with low Cl<sup>-</sup> solution are plotted in the inset of the graph. \*\* $P < 0.01$ . Error bars, SEM.  $n = 5$



To find out whether the progressive decrease can be seen on a single cell level, the response was tested under current clamp conditions with a potassium-based internal pipette solution. The membrane potential showed a repetitive, transient depolarizing response (corresponding to EPSPs), sometimes followed by action potentials. The latter occurred especially during the early phase of stimulation. Two action potentials are observed in the early phase of stimulation (Fig. 2c, arrow). During high-frequency stimulation, the baseline response showed a sustained, depolarizing membrane potential shift. This sustained depolarization decayed slowly toward the resting potential within a few hundreds of milliseconds after cessation of stimulation. However, sometimes it was followed by a gradual rise and a peak after a few tens of milliseconds from the end of stimulation, again slowly decaying to the resting level within a few seconds (see, for example, Fig. 1b of Tominaga et al. [55], which shows a membrane potential trace obtained with a sharp intracellular electrode). The apparent amplitude of the individual transient responses to each shock decreased with increase in the number of shocks (cf. closed arrow and open arrow in Fig. 2d;  $12.97 \pm 4.61$  mV to the first stimulation,  $4.61 \pm 1.35$  mV to the 40th stimulation;  $P < 0.05$ ,  $n = 4$ ). This corroborates the effect observed in optical recordings in that EPSP amplitude incrementally decreases in terms of electrophysiological recording as recorded under current clamp conditions.

To determine whether the decrease in membrane potential response was caused by decreased synaptic transmission, we examined membrane current responses under voltage-clamp conditions with Cs-based, low Cl<sup>-</sup> internal pipette solution ( $E_{Cl} = -73$  mV; Fig. 3). Please note that the reversal potential of GABA<sub>A</sub> receptors should be more positive than the  $E_{Cl}$  due to the possible contribution of other ion species such as HCO<sub>3</sub><sup>-</sup>. The EPSCs showed progressive decrease (Fig. 3a). EPSC to the first stimulation was significantly larger than that to the last stimulation ( $-95.98 \pm 15.21$  pA to the first stimulation,  $-10.82 \pm 1.07$  pA to the 40th stimulation at -70 mV,  $P < 0.001$ ,  $n = 5$ ,  $n$  means number of

cells). GABA<sub>A</sub> receptor antagonists reduce the amplitude of high-frequency stimulation-induced long-lasting depolarization [27, 44, 51, 53]. The long-lasting component of the current reversed its sign when the holding potential was brought to -30 from -70 mV (Fig. 3a, b; red and black trace, respectively). EPSCs superimposed on the long-lasting components also showed a progressive decrease in amplitude at depolarized holding potentials ( $-43.03 \pm 1.16$  pA to the first stimulation,  $-5.41 \pm 1.56$  pA to the 40th stimulation at -30 mV,  $P < 0.01$ ,  $n = 5$  cells). That is, the progressive

decrease shown in membrane potential changes, i.e., EPSP, are accompanied by a reduction in EPSC amplitudes.

Application of PiTX reduced the long-lasting tail current components (Fig. 3c, d), and the current did not show a reversal, even when the holding potential was brought to  $-30$  mV. The amplitude of the long-lasting tail current components (50 ms after cessation of the stimulation train) was plotted in Fig. 3e. The slope conductance calculated from these values was significantly different between control and PiTX application ( $4.73 \pm 0.99$  nS in control,  $0.36 \pm 0.25$  nS in PiTX,  $n=5$ ,  $P < 0.01$ ,  $n$  means number of cells). The reversal potential of the tail current recorded with the low  $\text{Cl}^-$  internal solution (black symbols in Fig. 3e) was shifted in positive direction if we used an internal solution with higher  $\text{Cl}^-$  concentration ( $E_{\text{Cl}^-} = -29$  mV). This observation supports the idea that the tail current components are primarily carried by  $\text{Cl}^-$ .

The individual EPSCs were not clearly distinguishable due to their longer duration in Fig. 3c. However, EPSCs did not show the progressive decrease as was observed under control condition (cf. Fig. 3b, d). We thought that the peak amplitude of EPSCs did not change during the period of burst stimulation so that the envelope of the response appeared to be square (Fig. 3c), even when the long-lasting tail was suppressed under PiTX. These results suggest that PiTX diminished the progressive decrease of EPSC.

#### Recovery of individual responses from incremental inhibition

During the tetanic stimulation, individual EPSPs are difficult to be isolated; hence, to study the progressive decrease of EPSPs clearer, we examined the recovery of EPSP amplitudes by probing with a single stimulus at various times after cessation of the standard tetanic stimulation. We probed the EPSP amplitude at 20, 50, 100, 200, and 500 ms after the tetanus ended, as shown in Fig. 4a. These single probe stimuli elicited responses (blue rectangular highlights) superimposed on the tail of the long-lasting depolarizing optical signal and on the long tail of the field potential shift (Fig. 4b, bottom).

The traces shown in Fig. 4c show the time course of incremental inhibition of EPSPs during tetanic stimulation and their recovery as a function of time from the beginning of the stimulation protocol; the long-lasting depolarizing component was subtracted out, as before. The amplitude of probe stimulus was significantly smaller than the control when the delay was smaller than 200 ms (delay  $< 50$  ms,  $P < 0.001$ ; delay 100 ms,  $P < 0.05$  at  $100 \mu\text{m}$  away from the stimulation site). The pooled data are shown in Fig. 4f.

The time course of the recovery in presence of PiTX was tested using the same probe stimuli (Fig. 4d). Since the individual EPSP was not isolated under PiTX, a trace

during the tetanic stimulation is shown in Fig. 4e. The response amplitudes to the delayed probe stimuli were somewhat smaller than the initial amplitude of the high-frequency responses (thin blue horizontal line; a and b in Fig. 4d), but they recovered soon (c in Fig. 4d). There were no significant differences in the amplitude of the response to the delayed probe stimuli compared to the control.

Figure 4f shows the pooled data of the amplitude of the probe signals relative to the control signal at different distances from the stimulation site in the control and in the presence of PiTX. In the control condition, the amplitude of the probe signals in the vicinity of the stimulation electrode (100 to  $300 \mu\text{m}$ ) was suppressed. The decreased response gradually recovered to the original level. In contrast, the response at distal areas (600 to  $900 \mu\text{m}$ ) showed significant transient facilitation after cessation of the tetanic stimulation. The distance-dependent decrease and facilitation of EPSPs was diminished by the application of PiTX. This finding is apparent in the three-dimensional plot shown in Fig. 4g. This can also be seen in the traces shown in Figs. 6a (control) and 7a (in the presence of PiTX).

Inhibition of the long-lasting  $\text{GABA}_A$ -dependent component and the relative insensitivity of the EPSP response amplitudes to delayed posttetanus probe stimuli suggests that the  $\text{GABA}_A$  antagonist PiTX also reversed, at least partially, the incremental inhibition of EPSPs.

#### Spatial convergence of the response and effect of PiTX on spatial convergence

The progressive decrease in EPSPs is one of the characteristics of tetanic burst stimulation-induced responses. A steep spatial dependence of the long-lasting depolarizing response amplitude is another characteristic [55]. In order to study the GABA-mediated modulation of depolarizing transmission and propagation in area CA1, we examined the spatial convergence of the response under standard conditions (control) and in the presence of PiTX.

The peak amplitude of the responses to tetanic stimulation in slices bathed in normal aCSF (control) and in aCSF containing PiTX is plotted as three-dimensional graphs in Fig. 5a. The response was only weakly convergent in the presence of PiTX. This difference is clearer in Fig. 5b, in which the two plots are re-color-coded and superimposed. The steep convergence of the response at the site of stimulation in the control condition (grayscale) was mostly absent when  $\text{GABA}_A$  receptors were pharmacologically antagonized, while the response amplitude in the distal parts of CA1 was fairly similar in the two conditions.

Representative traces showing the effect of PiTX on the optical signals at different pixels in SR are shown in Fig. 5c. The long-lasting depolarizing component was

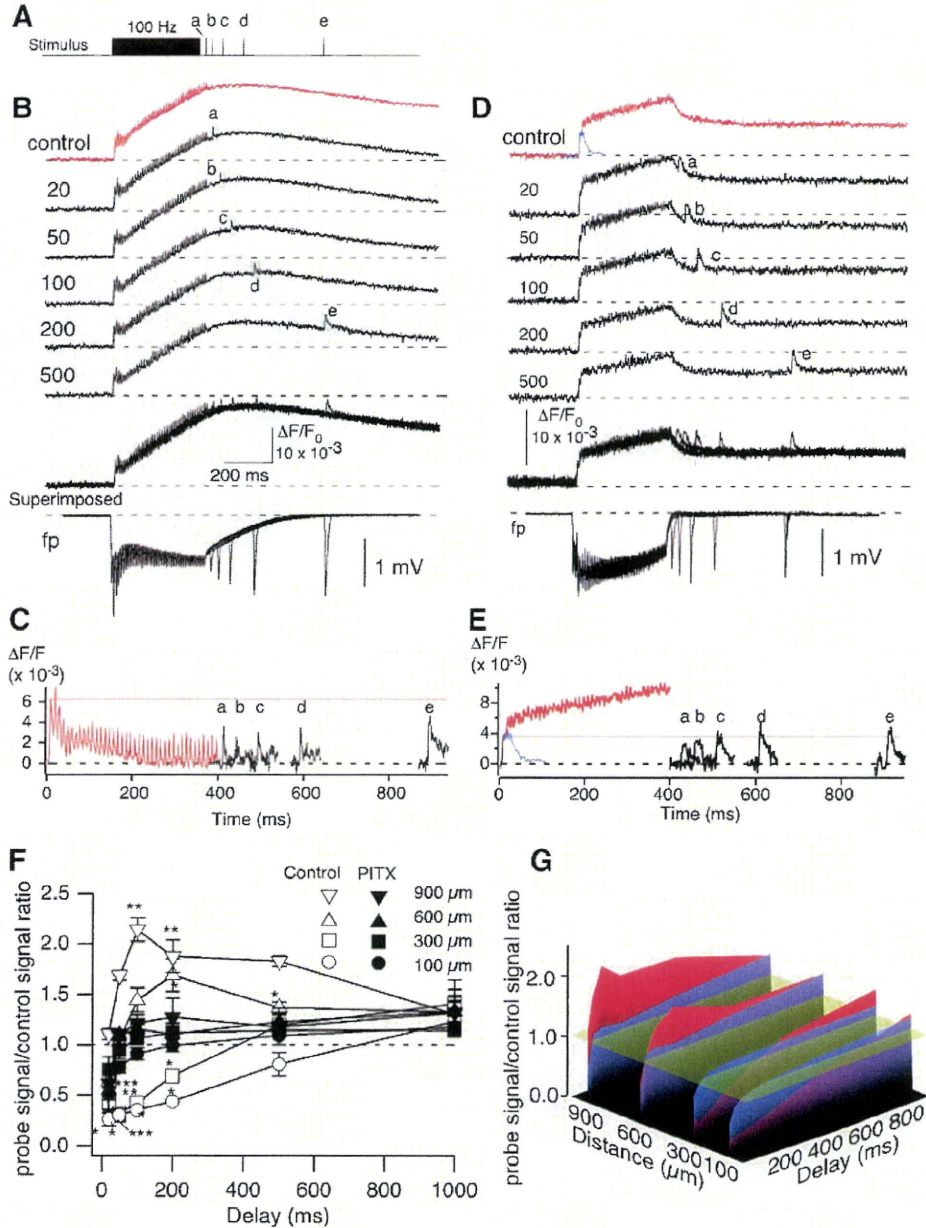
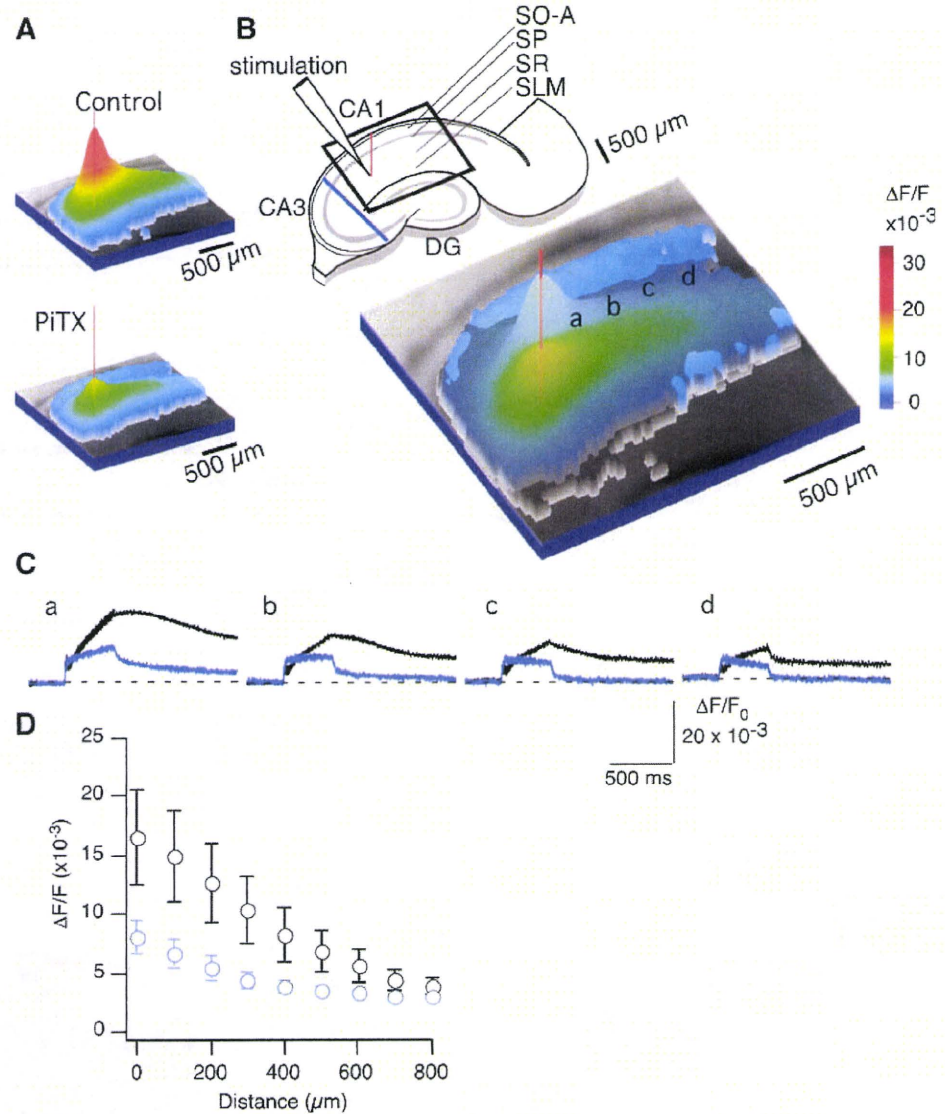


**Fig. 4** Recovery of EPSP amplitude after incremental inhibition in normal aCSF (**b, c**) and in the presence of the GABA<sub>A</sub> receptor antagonist PiTX (**d, e**). **a** Schematic drawing of stimulus timing. Delayed single stimuli used to probe EPSP amplitude after cessation of tetanic stimulation (20, 50, 100, 200, and 500 ms posttetanus delay) are shown in the same trace (**a–e**). **b** Representative trace of the optical signal recorded in response to tetanic stimulation (100 Hz, 40 pulses; *red line*; control) and variable-interval probe traces (**a–e**) obtained at the same pixel in response to a single stimulus. *Bottom trace* shows superimposed control and all probe traces of the optical signal and the corresponding field potential (*fp*) recorded in the middle of stratum radiatum. **c** Comparison of EPSP amplitudes in optical recordings after the long-depolarizing component was removed using the same subtraction method presented in Fig. 1. *Red trace* shows the resulting individual trace obtained during the tetanus, and the subsequent *black traces* show the resulting probe EPSPs traces, **a–e**, all as a function of time from the start of the high-frequency stimulation.

The probe responses were obtained by subtracting the control response (*red trace in b*) from the responses to probing episodes. Probe traces and traces recorded during the tetanus are drawn on same time scale. **d** The same responses as shown in **b** in the presence of PiTX. **e** Time course of the optical signal during tetanic stimulation in the presence of PiTX (*blue trace*) and the subtracted responses to delayed probe stimuli; same time scale. *Thin red horizontal line* shows the amplitude of the initial EPSP. **f** Pooled data of the amplitude of the probe signals relative to the control signal at points 100, 300, 600, and 900 μm away from the stimulation site in control solution (*open symbols*) and in the presence of PiTX (*filled symbols*). Time scale shows the delay from the cessation of tetanus. **g** Three-dimensional presentation of pooled data shown in **f**. The *red colored plots* show interpolated mean values of time course shown in the control solution. The *blue colored plots* show the time course in the presence of PiTX.

**Fig. 5** Inhibition of GABA<sub>A</sub> receptors reduces distance-dependent long-lasting depolarization. **a** Three-dimensional plots showing the maximum amplitudes of CA1 neuronal responses to tetanic stimulation (100 Hz, 40 pulses) in slices bathed in normal aCSF (control) and in aCSF containing 100  $\mu$ M PiTX. Amplitudes are mapped according to each corresponding pixel. Red vertical lines represent the stimulation site in the slice. **b** Superimposed three-dimensional plots for the control (grayscale) and PiTX (pseudocolored) conditions. A reference three-dimensional illustration represents the hippocampus, the stimulation electrode, and the field of view of the imaging system (square). SO-A stratum oriens–alveus, SP stratum pyramidale, SR stratum radiatum, SLM stratum lacunosum–moleculare. **c** Representative traces of the optical signal obtained from single pixels at various locations in stratum radiatum (a–d correspond to locations shown in **b**). Black traces show control responses, and blue traces show responses in the presence of PiTX. **d** Response peak amplitudes at the tail end of the responses, which were sampled 200 ms after the end of tetanic stimulation ( $n=4$ , control;  $n=4$ , PiTX). Error bars are SEM (see also Supplemental movie s3.mpg.)



effectively removed by application of PiTX, which is especially evident in distal parts of CA1 distal (toward the subiculum).

Summarized data are shown in Fig. 5d, in which the response amplitude measured at 200 ms from cessation of tetanic stimulation is plotted as a function of distance from the site of stimulation. Here, the averages of the tetanus-induced responses clearly demonstrate the effect of antagonizing CA1 GABA<sub>A</sub> receptors: The distribution of the response across a wide transverse area of the proximal part of the apical dendritic field of CA1 was attenuated and more uniformly excitatory. We conclude that the application of a GABA<sub>A</sub> receptor antagonist makes the distribution of the tetanus-induced response more uniform or flattens it (for an animated presentation of these findings, see Supplemental movie s5.mpg).

Enhanced propagation following tetanus-induced incremental inhibition of EPSPs

Next, we examined the effect of distance on the recovery of EPSP amplitude from incremental inhibition (Fig. 6) after tetanic stimulation. The traces in Fig. 6a show time- and distance-ordered traces of the optical signal in response to tetanic stimulation and to delayed probe stimuli delivered at various delays after the end of the tetanus (increasing delays, ordered top to bottom; increasing distance from stimulation site, ordered left to right). The probe responses were obtained by subtracting the control response (the response to high-frequency stimulation only, i.e., traces presented at 0 ms in a–d of Fig. 6a) from the responses to the probing episodes (traces presented at 20, 50, 100, 200, and 500 ms in a–d of Fig. 6a). Representative traces of the

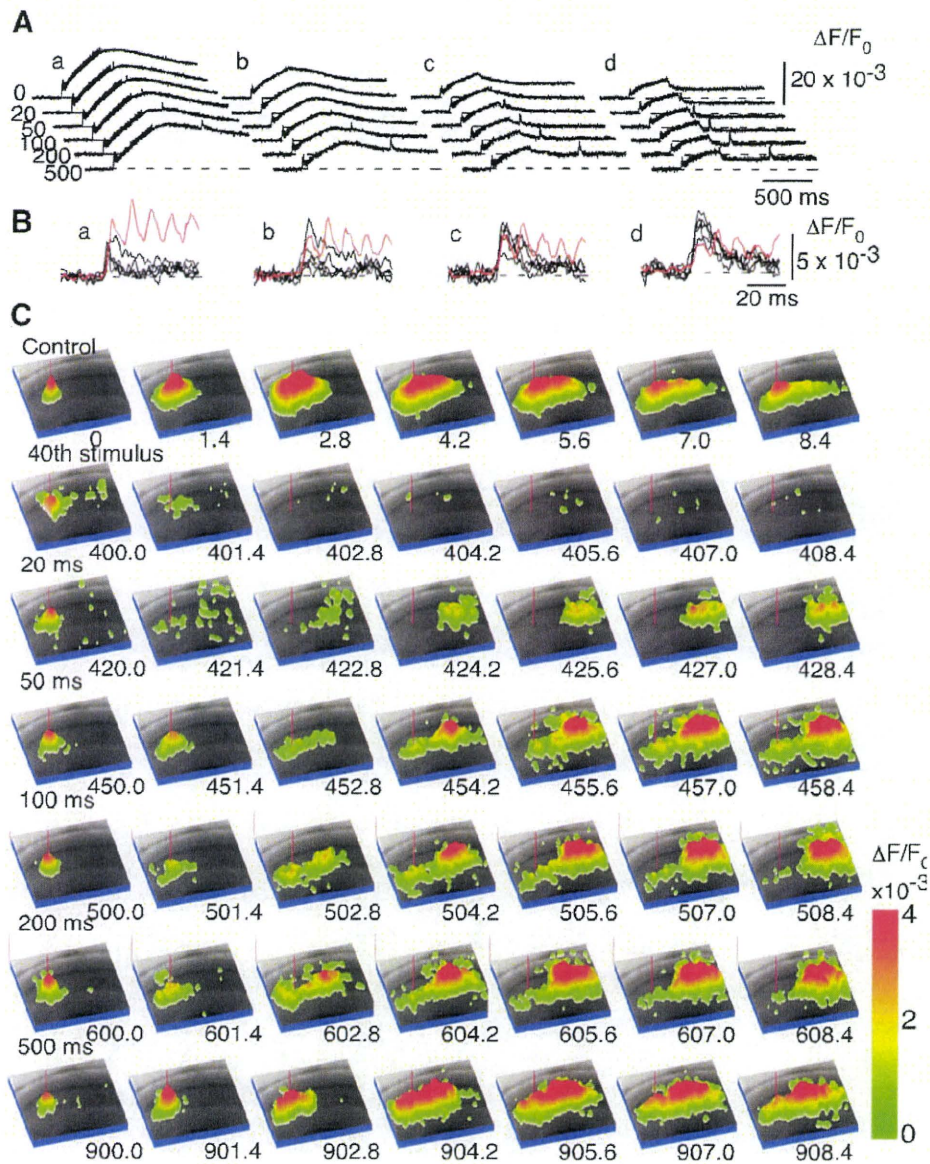


**Fig. 6** Distance-dependent inhibition and enhancement of EPSPs in CA1 of rat hippocampal slices after tetanic stimulation. **a** Representative traces of the optically detected neuronal responses elicited by tetanic stimulation (100 Hz, 40 pulses) and following single stimulation with various delays (20, 50, 100, 200, and 500 ms; 0 is no delay) from the end of the tetanic stimulation at various distances from the site of stimulation (*a* 200  $\mu\text{m}$ , *b* 400  $\mu\text{m}$ , *c* 600  $\mu\text{m}$ , and *d* 800  $\mu\text{m}$ ). Probe responses are visible as smaller, delayed, sharp depolarizations riding on the tail of the response. **b** Traces represent the probe responses after subtraction, which are displayed on expanded time and amplitude scales and aligned to the start of high-frequency stimulation. The red traces superimposed on the subtracted traces represent the initial phase of the

response to tetanus. **c** Consecutive three-dimensional plots show pseudocolored activity maps of the neural response as it appears in the optical signal. Red vertical lines represent stimulating electrode. The topmost row (control) shows the pattern of neuronal excitation propagation of the response to the first stimulus of the tetanic stimulation, displayed every 1.4 ms. The second row (40th pulse) shows the pattern of propagation with the last (40th pulse) stimulus, after subtraction of the long-lasting component. The subsequent rows show the propagation pattern of neuronal excitation to the delayed probe stimulus after the subtraction of the response by the control response at delays of 20, 40, 100, 200, and 500 ms, respectively (see also Supplemental movie s4.mpg.)

subtracted signals are superimposed and shown in a–d of Fig. 6b (a of Fig. 6a is the same trace shown in Fig. 4b.)

At a pixel near the stimulation site, the peak amplitudes of the responses to single probe stimuli delivered after cessation

of the tetanus were smaller than the responses to the first stimulus of the tetanic stimulation. These gradually recovered with increasingly long intervals, as before (a of Fig. 6a). On the other hand, at a pixel far from the stimulating site and at

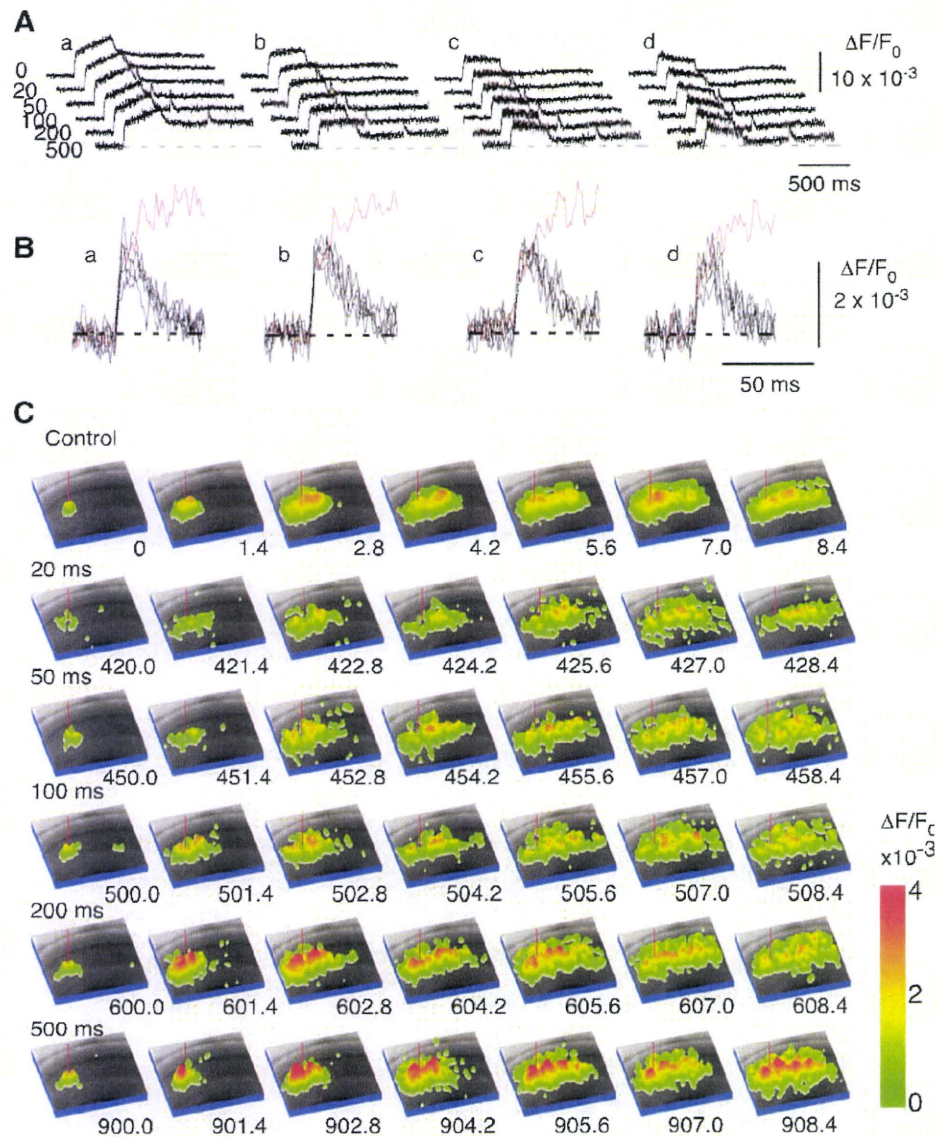


**Fig. 7** Antagonism of GABA<sub>A</sub> receptors “homogenizes” probe responses in spatial and time domains following tetanic stimulation. Experiments were conducted with 100  $\mu$ M PiTX in the slice chamber perfusate. The same high-frequency stimulation and delayed single probe stimulus protocol and subtraction procedure were used as in earlier experiments. **a** Representative traces of the optical signal recorded in stratum radiatum following the tetanus and the delayed posttetanus probe responses to single stimuli delivered at 20, 50, 100, 200, and 500 ms (ordered top to bottom, respectively) after the tetanus. Probe responses are visible as smaller, delayed, sharp depolarizations riding on the tail of the response. **b** Traces ordered left to right were obtained from individual pixels located at increasing

distances from the site of stimulation (*a* 200  $\mu$ m, *b* 400  $\mu$ m, *c* 600  $\mu$ m, and *d* 800  $\mu$ m). Lower traces represent the probe responses after subtraction. These are displayed on expanded time and amplitude scales and aligned to the start of high-frequency stimulation. The red traces superimposed on the subtracted traces represent the initial phase of the response to tetanus stimulation in the presence of PiTX. **c** Consecutive images of the optical signal amplitude showing the propagation of neuronal excitation in response to the first stimulus of the tetanus (first row; control) and those to the delayed probe stimuli. The red vertical lines on the images show the site of stimulation (1.4 ms/images; see also Supplemental movie s5.mpg)

short intervals, the probe response was slightly larger than its control and became even larger as the posttetanus probe intervals increased (d of Fig. 6b). As b and c of Fig. 6b illustrate, we observed an intermediate-sized effect at distances and intervals between these extremes.

Figure 6c shows the propagation pattern in terms of a time-lapsed three-dimensional image of the optical signal. The propagation of the response to the last stimulus (40th pulse) of the tetanus (second row, Fig. 6c) was far smaller than that to the first stimulus (first row, control). The

response for the latter case was confined almost entirely to the area immediately around the stimulating site. Twenty milliseconds after tetanus cessation, the propagation recovered a small amount from the inhibition (third row, Fig. 6c), especially at distal parts of CA1, far from the stimulating site. As the delay between tetanus cessation and probe stimulus increased, the distance-dependent recovery of the propagation got clearer. Moreover, the response clearly was enhanced distally with progressively more delayed probe stimuli. In other words, we observed time-dependent enhancement of neuronal activity propagation after high-frequency stimulation ended (for an animated presentation of these findings, see Supplemental movie s4.mpg).

The effect of PiTX on the distance-dependent recovery and enhancement of the response is shown in Fig. 7; the same delayed, single probe stimulus and subtraction protocol was used as in earlier experiments. As is clear in the subtracted traces of the probe responses (Fig. 7b), the response amplitudes did not change much, irrespective of the length of the delay or the distance from the stimulating site.

When comparing the three-dimensional plots of Fig. 6c (no PiTX) to those of Fig. 7c, it becomes especially clear that the pattern of response propagation in the presence of PiTX varies little between the control case (only tetanus, no probe stimuli) and the experimental case (tetanus plus probe stimuli). That is, the application of PiTX diminished the asymmetry of the typical tetanus-induced response in the space and time domains, approaching an overall uniformity of depolarization over a large area of the transverse plane of CA1.

## Discussion

Membrane potential responses to tetanic burst stimulation (100 Hz, 40 pulses) of Schaffer collateral afferents in CA1 of rat hippocampal slice preparations were examined by means of optical recording of membrane potentials as well as by conventional patch-clamp and field potential recordings. We demonstrated that burst stimulation caused a long-lasting depolarization observable in the optical signal near the stimulating site, which was accompanied by a progressive decrease in EPSP amplitude. In contrast, the long-lasting depolarization was weaker when the distance from the stimulation site was increased. However, after cessation of the tetanic stimulation, we observed subsequent facilitation of individual EPSPs for up to 1,000 ms in sites further than 600  $\mu\text{m}$ . The long-lasting depolarization and the progressive decrease and facilitation of EPSPs were diminished by application of PiTX and were thus dependent on GABA<sub>A</sub> receptors. Taking the voltage-clamp experiments (Fig. 3) into account, we hypothesize that this

intense stimulation causes spill over of GABA, which in turn induces long-lasting depolarization at the postsynaptic membrane. On studying a wider portion of CA1 using the optical-imaging method, we observed that the same stimulus facilitated excitation propagation and that this effect was dependent on GABA<sub>A</sub> receptors. A recent study showed enhanced activation of GABA<sub>A</sub> receptors after an acute perfusion of di-4-ANEPPS to cultured neurons [41]; however, we did not observe any qualitative difference in the physiology of slice preparations after the wash.

Synaptically released GABA causes long-lasting depolarization at the postsynaptic membrane

Blockage of the long-lasting depolarization by the GABA<sub>A</sub> receptor antagonist PiTX (Figs. 3, 4, and 5) is consistent with lines of evidence showing that high-frequency stimulation can induce sustained GABA<sub>A</sub> receptor-dependent depolarization under certain conditions [19, 27, 44, 51, 53]. The reversal of the long-lasting membrane current (Fig. 3a) corroborates this. This kind of depolarization is mostly caused by a depolarizing GABA<sub>A</sub> receptor response [1, 52] related to excess GABA accumulation.

It is widely accepted that the depolarizing GABA<sub>A</sub> receptor potential is mediated by a shift in the reversal potential of the GABA<sub>A</sub> receptor channel ( $E_{\text{GABA}}$ ), from hyperpolarizing to depolarizing, while the possible involvement of different types of extrasynaptic GABA<sub>A</sub> receptor channels [2] is still suspected. It is also accepted that the shift of  $E_{\text{GABA}}$  involves processes that mostly depend on a change in the intracellular  $\text{Cl}^-$  concentration caused by the changes in the extracellular ionic environment (mostly  $\text{HCO}_3^-$ ,  $\text{K}^+$ ,  $\text{Cl}^-$  ions) mediated by the high-frequency stimulation [27, 32, 34, 51, 53]; also see the recent reviews by [23, 43, 52].

Synaptically released GABA causes modulation of excitatory transmission

We have shown that a progressive decrease of EPSPs occurs in an area where the long-lasting depolarization was prominent (Figs. 1 and 2). We postulate that this area accumulates excess GABA (Fig. 5). Excess GABA may inhibit EPSPs directly through typical GABA<sub>A</sub> receptor actions at the postsynaptic cell, for example, shunting of excitatory current. However, we demonstrated incremental inhibition of EPSCs under voltage-clamp conditions (Fig. 3). The usual direct postsynaptic GABA<sub>A</sub> receptor actions cannot reduce EPSCs as we describe here. The reduced EPSCs may be attributable to disruption of space-clamp condition due to massively reduced input conductance by GABA<sub>A</sub> receptors. However, it is not clear that to what extent this can affect to the amplitude of the EPSCs. A

complete reversal of the long-lasting current on the depolarized holding potential may indicate that the membrane potential is still under the control of the voltage-clamp condition, at least at the site where the GABA<sub>A</sub> receptors are functional; thus, disruption of the space-clamp condition would not have a considerable effect on the amplitude of the EPSCs. In addition, the time course of the EPSC, which should be altered under a disrupted space-clamp condition, did not change to a great extent, even at the end of the train of stimulation. This may reduce the feasibility of the effect of disruption of the space-clamp condition on EPSCs. It is also not feasible to postulate unknown postsynaptic crosstalk between GABA<sub>A</sub> receptor activation and glutamate receptors because even at a depolarizing holding potential, we observed the progressive decrease of EPSCs. In addition, because GABA<sub>A</sub> receptor antagonists diminish the progressive decrease, presynaptic neurotransmitter depletion cannot account for the progressive decrease.

Alternatively, we postulate that direct GABA<sub>A</sub> receptor-mediated inhibition of excitatory synaptic transmission accounts for the progressive decrease of EPSPs. Presynaptic GABA<sub>A</sub> receptor-mediated modulation of synaptic transmission has been observed in many areas of the CNS, following its first description in the spinal cord [21, 22]. It has also been found to occur at mossy fiber synapses in hippocampal CA3 [30, 31, 45].

Activation of presynaptic GABA<sub>A</sub> receptors can modulate glutamate release in downward [45] and upward [30] directions. Hence, it is reasonable to propose that the activation of presynaptic GABA<sub>A</sub> receptors is the cause of the incremental inhibition and also the subsequent facilitation of propagation of excitation shown in this study. The other possible explanation could be conduction block of axons caused by axonal GABA<sub>A</sub> receptors [59]. It is interesting to point out that in Fig. 1d, the presynaptic fiber activity seemed to be decreased somewhat compared to that recorded in low Ca<sup>2+</sup> solution. The mechanism underlying this finding may involve elevation of extracellular K<sup>+</sup> levels [34] by sustained depolarization of postsynaptic neurons, which in turn induces conduction blockage of the presynaptic axonal fibers [55]. However, it remains unclear whether this hypothesis accounts for the dramatic decrease in postsynaptic response (Fig. 1b).

Plausible mechanisms of the late “super recovery” or response facilitation

Response enhancement following high-frequency stimulation may be posttraumatic hyperexcitability [46], tetanic stimulation-induced gamma- and beta-band oscillations [10, 58, 62] and seizure-like activity [25, 29], and/or posttetanic

potentiation. The mechanisms of these augmented kinds of excitability induced by high-frequency stimulation remain unclear, as far as we know. However, it is interesting to note that the enhancement after the tetanus in the present experiment was more prominent at progressively more distal sites in the transverse axis of CA1 (i.e., toward the subiculum), regions where the long-lasting depolarization was not prominent and/or the incremental inhibition was prominent. The response at a distance of 300 μm from the site of tetanus application showed enhancement only after 20 ms or more elapsed since the end of the tetanus, while inhibition was still prominent at more proximal sites (toward the stimulating electrode at the CA3–CA1 border). The late “super recovery” of EPSPs at distant sites from the stimulation electrode as well as the transient decrease of EPSPs at proximal sites was sensitive to PiTX. Thus, the opposite short-term modulations of excitatory transmission were both dependent on activation of GABA<sub>A</sub> receptors. We propose a balance between inhibitory and facilitative action of excess GABA accumulation: At higher concentrations, excess GABA accumulation may inhibit neural signal transduction, whereas at lower concentrations, it may facilitate neural signal transduction, possibly by different mechanisms. Transient weakening of inhibition due to transient reversal of membrane potential response [8] may account for the late “super recovery”. The same electrical stimulation can recruit a short-term GABAergic spatially differentiated modulation in neural circuits when it was encoded into a 100-Hz tetanic stimulation. This may highlight the GABAergic action in frequency-dependent neuronal signal processing.

Physiological implication of the tetanus-induced response changes in space and time

The tetanic stimulation used in the present study is one of the most common stimulation protocols used to induce LTP, and indeed, it mimics hippocampal pyramidal cell bursting observed during learning behavior [64]. The incremental inhibition of excitation propagation we observed during tetanic afferent stimulation is important for understanding more clearly the neural basis of information processing that presumably is embedded in neuronal bursting [12, 14, 28, 63]. The powerful influence of the GABA circuitry in shaping the patterns of CA1 excitatory activity in response to tetanic stimulation in space and time domains demonstrated here suggests that external influences on this GABA circuitry will have a profound impact on bursting-mediated information flow through the hippocampus. GABA<sub>A</sub> receptor-dependent inhibition would also be an important stabilizing factor for GABA<sub>A</sub> receptor-dependent synchronized activity mediated by the interneuron network of hippocampus [49].



The steep spatial convergence of GABA<sub>A</sub> receptor-dependent heterogenic progressive decrease and facilitation of EPSP (Figs. 4, 5, 6 and 7) would also be important to shaping heterogenic LTP induction [16, 56]. The subsequent enhancement of EPSP at distal portion can also account for the heterogenic induction of LTP.

To our knowledge, little is known about the presynaptic GABA<sub>A</sub> receptor-mediated modulation of glutamatergic synaptic transmission in the Schaffer collateral pathway of area CA1. If the present incremental inhibition does indeed occur in behaving animals, then it would represent a new aspect of GABA-mediated modulation of information flow through and beyond area CA1 of the hippocampus.

**Acknowledgments** We thank Dr. Michinori Ichikawa for his kind encouragement and help during the early phase of this work and Dr. Michael E. Barish for his critical comments on an earlier version of the manuscript.

## References

- Alger BE, Nicoll RA (1979) GABA-mediated biphasic inhibitory responses in hippocampus. *Nature* 281:315–317
- Alger BE, Nicoll RA (1982) Pharmacological evidence for two kinds of GABA receptor on rat hippocampal pyramidal cells studied in vitro. *J Physiol (Lond)* 328:125–141
- Ang CW, Carlson GC, Coulter DA (2006) Massive and specific dysregulation of direct cortical input to the hippocampus in temporal lobe epilepsy. *J Neurosci* 26:11850–11856
- Bai L, Huang X, Yang Q, Wu JY (2006) Spatiotemporal patterns of an evoked network oscillation in neocortical slices: coupled local oscillators. *J Neurophysiol* 96:2528–2538
- Bartos M, Vida I, Jonas P (2007) Synaptic mechanisms of synchronized gamma oscillations in inhibitory interneuron networks. *Nat Rev Neurosci* 8:45–56
- Beau FENL, Alger BE (1998) Transient suppression of GABA<sub>A</sub>-receptor-mediated IPSPs after epileptiform burst discharges in CA1 pyramidal cells. *J Neurophysiol* 79:659–669
- Ben-Ari Y, Gaiarsa JL, Tyzio R, Khazipov R (2007) GABA: a pioneer transmitter that excites immature neurons and generates primitive oscillations. *Physiol Rev* 87:1215–1284
- Blaesse P, Airaksinen MS, Rivera C, Kaila K (2009) Cation-chloride cotransporters and neuronal function. *Neuron* 61:820–838
- Bliss TVP, Collingridge GL (1993) A synaptic model of memory: long-term potentiation in the hippocampus. *Nature* 361:31–39
- Bracci E, Vreugdenhil M, Hack SP, Jefferys JG (1999) On the synchronizing mechanisms of tetanically induced hippocampal oscillations. *J Neurosci* 19:8104–8113
- Broicher T, Bidmon H-J, Kamuf B, Coulon P, Gorji A, Pape H-C, Speckmann E-J, Budde T (2010) Thalamic afferent activation of supragranular layers in auditory cortex in vitro: a voltage sensitive dye study. *Neuroscience* 165:371–385
- Buzsaki G, Horvath Z, Urioste R, Hetke J, Wise K (1992) High-frequency network oscillation in the hippocampus. *Science* 256:1025–1027
- Buzsaki G, Leung LW, Vanderwolf CH (1983) Cellular bases of hippocampal EEG in the behaving rat. *Brain Res* 287:139–171
- Buzsaki G, Penttonen M, Nadasdy Z, Bragin A (1996) Pattern and inhibition-dependent invasion of pyramidal cell dendrites by fast spikes in the hippocampus in vivo. *Proc Natl Acad Sci USA* 93:9921–9925
- Carriero G, Uva L, Gnatkovsky V, de Curtis M (2009) Distribution of the olfactory fiber input into the olfactory tubercle of the in vitro isolated guinea pig brain. *J Neurophysiol* 101:1613–1619
- Chang PY, Jackson MB (2006) Heterogeneous spatial patterns of long-term potentiation in rat hippocampal slices. *J Physiol* 576:427–443
- Cohen LB, Salzberg BM (1978) Optical measurement of membrane potential. *Rev Physiol Biochem Pharmacol* 83:35–88
- Coulter DA, Carlson GC (2007) Functional regulation of the dentate gyrus by GABA-mediated inhibition. *Prog Brain Res* 163:235–243
- Davies CH, Collingridge GL (1993) The physiological regulation of synaptic inhibition by GABA<sub>B</sub> autoreceptors in rat hippocampus. *J Physiol* 472:245–265
- de Curtis M, Takashima I, Iijima T (1999) Optical recording of cortical activity after in vitro perfusion of cerebral arteries with a voltage-sensitive dye. *Brain Res* 837:314–319
- Dudel J, Kuffler SW (1961) Presynaptic inhibition at the crayfish neuromuscular junction. *J Physiol* 155:543–562
- Eccles JC, Schmidt R, Willis WD (1963) Pharmacological studies on presynaptic inhibition. *J Physiol* 168:500–530
- Farrant M, Kaila K (2007) The cellular, molecular and ionic basis of GABA(A) receptor signalling. *Prog Brain Res* 160:59–87
- Fries P, Nikolic D, Singer W (2007) The gamma cycle. *Trends Neurosci* 30:309–316
- Fujiwara-Tsukamoto Y, Isomura Y, Imanishi M, Fukai T, Takada M (2007) Distinct types of ionic modulation of GABA actions in pyramidal cells and interneurons during electrical induction of hippocampal seizure-like network activity. *Eur J Neurosci* 25:2713–2725
- Grinvald A, Hildesheim R (2004) VSDI: a new era in functional imaging of cortical dynamics. *Nat Rev Neurosci* 5:874–885
- Grover LM, Lambert NA, Schwartzkroin PA, Teyler TJ (1993) Role of HCO<sub>3</sub><sup>-</sup> ions in depolarizing GABA<sub>A</sub> receptor-mediated responses in pyramidal cells of rat hippocampus. *J Neurophysiol* 69:1541–1555
- Harris KD, Hirase H, Leinekugel X, Henze DA, Buzsaki G (2001) Temporal interaction between single spikes and complex spike bursts in hippocampal pyramidal cells. *Neuron* 32:141–149
- Isomura Y, Fujiwara-Tsukamoto Y, Takada M (2003) Glutamatergic propagation of GABAergic seizure-like after discharge in the hippocampus in vitro. *J Neurophysiol* 90:2746–2751
- Jang IS, Ito Y, Akaike N (2005) Feed-forward facilitation of glutamate release by presynaptic GABA(A) receptors. *NeuroReport* 135:737–748
- Jang IS, Nakamura M, Ito Y, Akaike N (2006) Presynaptic GABA<sub>A</sub> receptors facilitate spontaneous glutamate release from presynaptic terminals on mechanically dissociated rat CA3 pyramidal neurons. *NeuroReport* 138:25–35
- Kaila K, Lamsa K, Smirnov S, Taira T, Voipio J (1997) Long-lasting GABA-mediated depolarization evoked by high-frequency stimulation in pyramidal neurons of rat hippocampal slice is attributable to a network-driven, bicarbonate-dependent K<sup>+</sup>-transient. *J Neurosci* 17:7662–7672
- Kaila K, Voipio J (1987) Postsynaptic fall in intracellular pH induced by GABA-activated bicarbonate conductance. *Nature* 330:163–165
- Kaila K, Voipio J, Paalasmaa P, Pasternack M, Deisz RA (1993) The role of bicarbonate in GABA<sub>A</sub> receptor-mediated IPSPs of rat neocortical neurones. *J Physiol* 464:273–289
- Kajiwara R, Takashima I, Mimura Y, Witter MP, Iijima T (2003) Amygdala input promotes spread of excitatory neural activity from perirhinal cortex to the entorhinal-hippocampal circuit. *J Neurophysiol* 89:2176–2184

36. Kajiwara R, Tominaga T, Takashima I (2007) Olfactory information converges in the amygdaloid cortex via the piriform and entorhinal cortices: observations in the guinea pig isolated whole-brain preparation. *Eur J Neurosci* 25:3648–3658
37. Kintoshi T, Ikeda H, Murase K (2010) Long-term potentiation of neuronal excitation in the central nucleus of the rat amygdala revealed by imaging with a voltage-sensitive dye. *Brain Res* 1349C:32–34
38. Koganezawa N, Taguchi A, Tominaga T, Ohara S, Tsutsui K, Witter MP, Iijima T (2008) Significance of the deep layers of entorhinal cortex for transfer of both perirhinal and amygdala inputs to the hippocampus. *Neurosci Res* 61:172–181
39. Mann EO, Suckling JM, Hajos N, Greenfield SA, Paulsen O (2005) Perisomatic feedback inhibition underlies cholinergically induced fast network oscillations in the rat hippocampus in vitro. *Neuron* 45:105–117
40. Mann EO, Tominaga T, Ichikawa M, Greenfield SA (2005) Cholinergic modulation of the spatiotemporal pattern of hippocampal activity in vitro. *Neuropharmacology* 48:118–133
41. Mennerick S, Chisari M, Shu HJ, Taylor A, Vasek M, Eisenman LN, Zorumski CF (2010) Diverse voltage-sensitive dyes modulate GABA<sub>A</sub> receptor function. *J Neurosci* 30:2871–2879
42. Paulsen O, Sejnowski TJ (2006) From invertebrate olfaction to human cognition: emerging computational functions of synchronized oscillatory activity. *J Neurosci* 26:1661–1662
43. Payne JA, Rivera C, Voipio J, Kaila K (2003) Cation-chloride cotransporters in neuronal communication, development and trauma. *Trends Neurosci* 26:199–206
44. Perreault P, Avoli M (1989) Effects of low concentrations of 4-aminopyridine on CA1 pyramidal cells of the hippocampus. *J Neurophysiol* 61:953–970
45. Ruiz A, Fabian-Fine R, Scott R, Walker MC, Rusakov DA, Kullmann DM (2003) GABA<sub>A</sub> receptors at hippocampal mossy fibers. *Neuron* 39:961–973
46. Santhakumar V, Voipio J, Kaila K, Soltesz I (2003) Post-traumatic hyperexcitability is not caused by impaired buffering of extracellular potassium. *J Neurosci* 23:5865–5876
47. Sejnowski TJ, Paulsen O (2006) Network oscillations: emerging computational principles. *J Neurosci* 26:1673–1676
48. Sinha SR, Saggau P (1999) Optical recording from populations of neurons in brain slices. In: Windhorst U, Johansson H (eds) *Modern techniques in neuroscience research*. Springer, Berlin, p 459–486
49. Sinha SR, Saggau P (2001) Imaging of 4-AP-induced, GABA<sub>A</sub>-dependent spontaneous synchronized activity mediated by the hippocampal interneuron network. *J Neurophysiol* 86:381–391
50. Staley KJ, Proctor WR (1999) Modulation of mammalian dendritic GABA<sub>A</sub> receptor function by the kinetics of Cl<sup>-</sup> and HCO<sub>3</sub><sup>-</sup> transport. *J Physiol Lond* 519:693–712
51. Staley KJ, Soldo BL, Proctor WR (1995) Ionic mechanisms of neuronal excitation by inhibitory GABA<sub>A</sub> receptors. *Science* 269:977–981
52. Stein V, Nicoll RA (2003) GABA generates excitement. *Neuron* 37:375–378
53. Taira T, Lamsa K, Kaila K (1997) Posttetanic excitation mediated by GABA<sub>A</sub> receptors in rat CA1 pyramidal neurons. *J Neurophysiol* 77:2213–2218
54. Tominaga T, Tominaga Y, Ichikawa M (2001) Simultaneous multi-site recordings of neural activity with an inline multi-electrode array and optical measurement in rat hippocampal slices. *Pflügers Arch Eur J Physiol* 443:317–322
55. Tominaga T, Tominaga Y, Ichikawa M (2002) Optical imaging of long-lasting depolarization on burst stimulation in area CA1 of rat hippocampal slices. *J Neurophysiol* 88:1523–1532
56. Tominaga T, Tominaga Y, Yamada H, Matsumoto G, Ichikawa M (2000) Quantification of optical signals with electrophysiological signals in neural activities of Di-4-ANEPPS stained rat hippocampal slices. *J Neurosci Methods* 102:11–23
57. Tominaga Y, Ichikawa M, Tominaga T (2009) Membrane potential response profiles of CA1 pyramidal cells probed with voltage-sensitive dye optical imaging in rat hippocampal slices reveal the impact of GABA<sub>A</sub>-mediated feed-forward inhibition in signal propagation. *Neurosci Res* 64:152–161
58. Traub RD, Whittington MA, Stanford IM, Jefferys JGR (1996) A mechanism for generation of long-range synchronous fast oscillations in the cortex. *Nature* 383:621–624
59. Trigo FF, Marty A, Stell BM (2008) Axonal GABA<sub>A</sub> receptors. *Eur J Neurosci* 28:841–848
60. Tu B, Gu Z, Shen JX, Lamb PW, Yakel JL (2009) Characterization of a nicotine-sensitive neuronal population in rat entorhinal cortex. *J Neurosci* 29:10436–10448
61. Voipio J, Kaila K (2000) GABAergic excitation and K<sup>(+)</sup>-mediated volume transmission in the hippocampus. *Prog Brain Res* 125:329–338
62. Whittington MA, Stanford IM, Colling SB, Jefferys JGR, Traub RD (1997) Spatiotemporal patterns of gamma frequency oscillations tetanically induced in the rat hippocampal slice. *J Physiol Lond* 502:591–607
63. Wu JY, Guan L, Tsau Y (1999) Propagating activation during oscillations and evoked responses in neocortical slices. *J Neurosci* 19:5005–5015
64. Ylinen A, Bragin A, Nadasdy Z, Jando G, Szabo I, Sik A, Buzsáki G (1995) Sharp wave-associated high-frequency oscillation (200–Hz) in the intact hippocampus—network and intracellular mechanisms. *J Neurosci* 15:30–46

理論/実験 技術

# 実践! 膜電位感受性色素による神経回路解析

富永貴志<sup>1,2</sup>, 富永洋子<sup>1</sup>

<sup>1</sup>徳島文理大学香川薬学部

<sup>2</sup>理化学研究所脳科学総合研究センター

## 1. はじめに

1966年の映画「ミクロの決死圏」では、小さくなって体の中を探検する科学者ら一行が、脳に到着して、神経細胞が軸索を走る光のパルスで情報のやり取りするさまを目の当たりにした。彼らが見たように、神経細胞同士が脳内で情報が伝えられるさまを眼で見られたら…。ヒトの脳が140億個もの神経細胞からできているのに、現在の最新のPC用CPU（インテル Core i7）でも、そのトランジスタ数がたった10億個程度であることを考えれば、これが脳の研究者の自然な欲求であることが理解できよう。この情報処理装置（CPU/脳）のはたらきを理解するためには1個1個の素子（トランジスタ/神経細胞）の動作のみならず、回路としての活動を目に見える形で知りたいのだ。ここでは、それを実現する手法の1つとして、膜電位感受性色素（Voltage Sensitive Dye; VSD）という特殊な色素分子による神経活動の可視化について解説する。今回は特に学部の実習のレベルでも実行可能な「容易な」技術となり得たことを紹介したい。

## 2. 光計測コトハジメ

神経細胞は、細胞膜内外の電位差（膜電位）の変化（神経興奮）という形で情報を伝えるので、その様は眼で見ることにはできない。しかし、神経興奮に伴って複屈折性や光散乱などの光学的性質に微小な変化（ $10^{-3}$ - $10^{-6}$ ）が生じることは、1950年代から知られていた。膜電位変化をよりよく「見る」ために、ウッズホール海洋生物学研究所（MBL）の田崎一二らは蛍光共鳴エネルギー移動法（FRET）を用いて、この光学信号を増幅して計測した<sup>1)</sup>。同研究所のLarry Cohenらのグループは、これをさらに発展させ、積極的に神経細胞の電気的信号を光学計測する色素の開発を行った<sup>2)</sup>。これら1970年頃の研究が、現在の光計測の基

礎となっている。

一般に細胞の膜電位は、ガラス微小電極のような電極を細胞膜へ刺して（あるいはくっつけて）細胞内の内液と電極内の電解質溶液を接触させ、そこから信号を取り出して増幅器で増幅して観測する。この電気生理学的手法の欠点は、電極の数を増やせないことであ

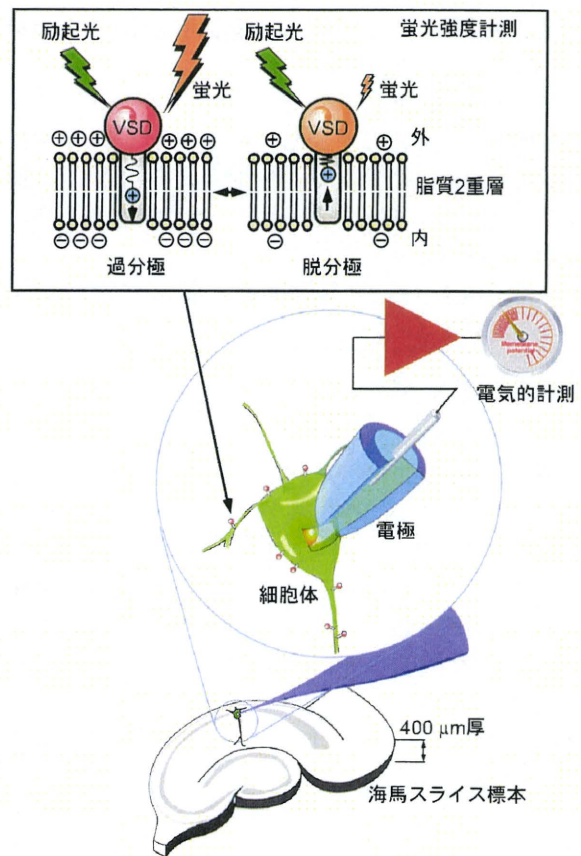


図1 脳海馬スライス標本における膜電位感受性色素（VSD）による計測（蛍光強度計測）と電極による計測（電気的計測）の模式図。VSDの蛍光は膜内の電界強度に依存して変化する。（電子ジャーナルではカラー）

Practices for the VSD Optical Recording Method of Neuronal Circuit Analysis

Takashi TOMINAGA<sup>1,2</sup> and Yoko TOMINAGA<sup>1</sup>

<sup>1</sup>Dept. Neurophysiol. Kagawa School of Pharmaceutical Sciences, Tokushima Bunri University

<sup>2</sup>Brain Science Institute, RIKEN

る。電極の大きさ、マニピュレータの配置などの制約のためである。一方、光計測では、細胞膜の脂質2重層に埋まって、膜を介した電界強度に応じた蛍光を生じる膜電位感受性色素の蛍光強度変化を計測する。そのため細胞や組織の各部位の電位変化を同時に計測することが可能である。

光計測には、高速・低雑音の特殊な撮像装置が必要である。日本では、東京医科歯科大学の神野耕太郎らのグループが独自の撮像装置を開発していた。また、電子技術総合研究所では松本元が、市川道教、飯島敏夫らを中心としたグループを率いて、市販化を念頭に精力的に撮像装置の開発を行った。このときに開発された浜松ホトニクス（株）製や、富士写真フィルム（株）製の撮像装置を、研究室にもっておられる方も多いのではないだろうか。海外では、Cohen や Grinvald ら研究者が早くから起業して光計測用撮像装置、色素を開発販売して普及させた。

一種の夢の技術が完成したと期待された当時の雰囲気を感じていらっしゃる方も多いだろう<sup>3)5)</sup>。膜電位感受性色素の一般の研究室での使用はその期待と高揚感の高さからいうと少し遅れて、21世紀に入ってから急速に使用され始めたようである<sup>6)</sup>。この後のセクションではこの遅れの原因となった技術的障壁のいくつかを解説したい。

### 3. 難しくしていたのはこれだ

#### 3.1 光計測の困難さ—明るいのに暗い像

膜電位感受性色素の膜電位変化に対する応答は、よくて $10^{-4}$ から $10^{-3}$ 程度（変化率）である。これは、カルシウム測光などで得られる信号サイズ（数十%から数百%）に比べるとたいへん小さい。また、神経細胞の活動に追従するためには、高速撮像が必須である。1ミリ秒から0.1ミリ秒の撮像速度（フレームレート）で計測できることが求められる。この精度（S/N値 $>60-70$  dB）でこのフレームレートを実現する必要があるわけである。

変化率が小さいので、光の粒子性から生じる問題もある。n個の光粒子の数を数えるのに、 $\sqrt{n}$ 個のエラーが確率的に生じる。光強度変化が $10^{-3}$ 程度のものとしたら、 $\sqrt{n}/n$ が $10^{-3}$ を超える必要があり、最低でも $10^6$ 個の光量子がいることになる。光計測に必要な撮像速度（だいたい1000フレーム毎秒）で、 $25\ \mu\text{m}$ 四方の撮像素子で計測すると、1つの撮像素子で $10^6$ の光量子数になる光（約 $10\ \mu\text{W}/\text{mm}^2$ ）はかなり強い。結像面に葉包紙などをかざすと、特に暗室でなくとも像が裸眼で見える程度である。このよう

に、他の蛍光測光などに携わっておられる方からすると感覚的には十分「明るい」画像も、光計測には「暗い」画像ということになる。

#### 3.2 光源—安定で明るい光源がない

光計測ではなるべく「明るい」像を得ることが必要になるので明るい光源が求められる。顕微鏡光源によく用いられるレーザー、高圧水銀灯、キセノンといった光源はミリ秒の世界では安定でない。レーザーでは数%のノイズとスペckルノイズ、高圧水銀灯、キセノンでは、火花（アーク）のゆらぎから生じるノイズが問題となる。そこで、（仕方なく）ハロゲン光源が一般的に用いられてきた。フィラメントの関係で150 W程度ハロゲン電球が最適といわれている。最近になって、ハイパワーのLEDが使用できるようになってきた。LEDは自己発熱に対する補正回路がついたものを選ぶ必要がある。

#### 3.3 光学系—低倍で明るいものが必要だ

神経回路の機能解析のためには、神経回路そのものの大きさ（たとえば海馬の1領野や大脳皮質のカラム構造は $500\ \mu\text{m}$ 四方程度）からいって総合倍率で1倍からせいぜい5倍までの光学倍率を選定する必要がある。この倍率で使える「明るい」落射蛍光顕微鏡がなかった。一般の生理の実験で使う正立顕微鏡で選べる対物レンズは（当時は）明るいものではなかった。倍率では、通常、実体顕微鏡が使われる領域になるが、適当なものがなくわれわれは独自の光学系を作成した。

#### 3.4 機械的なノイズ—ほんのわずかな振動が

$10^{-3}$ 以下の安定性が必要なので、機械的なノイズも問題になる。振動で像が動く場合、像のもともとの光強度の不均一性に応じた大きなノイズ（～数十%）を捨てる。ここで扱っている脳スライス標本からの光計測では、最も問題になるのは灌流液の水面の振動、スライス標本自体の動きである。

#### 3.5 膜電位感受性色素の選択

膜電位感受性色素には大きく分けて、吸光度の変化を生じさせるものと、蛍光強度の変化を生じさせるものがある。吸光度の変化の場合、明るい像を得ることが比較的容易であるが、変化量を規格化することが困難である。蛍光色素は、光強度を規格化することで、比較的定量的な計測が可能となる。一方で、蛍光強度は比較的弱く光学系に工夫が必要である。

実験に使用する組織に応じて色素を選ぶ必要がある。スライス標本では、吸光色素のRH-155は水溶性が高く染色はしやすいが、洗い流されやすく長期間の計測には向かなかった。またグリア細胞の信号を強く検出する傾向がみられた。蛍光色素のRH-795も水溶

性が高く、長期の計測には不適であるが、*in vivo* の標本に適している。スライス標本では、溶けにくい洗い流されにくい Di-4-ANEPPS が最適だった<sup>7)</sup>。最近、ANNINE-6 に注目しているがまだよい結果は得られていない。また、細胞内からの単一細胞染色には Di-2-ANEPEQ (JPW114) を用いる。

#### 4. 実際の応用例を少し

われわれは独自の光学系、後述するチャンパーシステム、ソフトウェアを開発して、定量的に光計測信号を扱えることを実証した<sup>7)</sup> (図2)。これらを使ってトランスジェニック動物のアッセイや治療薬のシーズのアッセイを行うなどのことも可能になった<sup>8)</sup>。また、テタヌス刺激が GABA(A) 受容体を介した短期可塑性を引き起こすことなどを明らかにした<sup>9)</sup>。また、活きた脳を取り出してその神経活動を計測することにも使われるようになってきた<sup>10)</sup>。

#### 5. 実習でも使える小型システムの開発

誰でも光計測を使って脳神経の活動を測れるようになれば、光計測のもつもとの網羅性から、脳神経の病気やそれに対する薬をより早くアッセイできるに違いない。そこで、誰でも使えることを目標にシステムを構築した (図3)。

##### 5.1 スライスチャンパー

脳スライス標本は、脳の神経回路機構を探るための非常に重要な標本である。しかし、この厚さ 400  $\mu\text{m}$  しかないフワフワして繊細なスライス標本の「生き」(生理学的な活性)を保ったまま取り扱うことはなかなか難しいことである。そこで、脳スライス標本を取り扱う器具に工夫を加え、スライス標本の取り扱いを容易にした<sup>7)</sup> (図3上;特許 3405301号, US 6448063)。この器具はスライス標本を保持する保持具と、実験時

に生理的塩溶液を還流するための実験槽からなる。スライス標本の保持具は、アクリル樹脂のリングにミリポア社のメンブレンフィルター (OMNIPORE MEMBRANE FILTERS, 0.45  $\mu\text{m}$ ; JHWP01300) を貼りつけたものである。スライス標本はフィルターに張り付くので、このリングをもって操作できる。このフィルターは、ガスや生理塩溶液の良好な交換を可能とする。また、実験槽にはリングごと嵌め込むことで固定でき「重石」などがなくとも、スライス標本が動いてしまう心配はない。また、色素で染色する際、1枚あたり約 100  $\mu\text{l}$  の染色液で染色できるので高価な膜電位感受性色素を節約できる。さらに、この実験槽は目視のパッチクランプ実験にも用いることができ、筆者は 400  $\mu\text{m}$  厚のスライス標本でも斜光を使い良好に実験を行うことができています。

##### 5.2 光学系

光計測には、強い蛍光が必要である。先に述べたように適当な光学系がないことからわれわれは独自の光

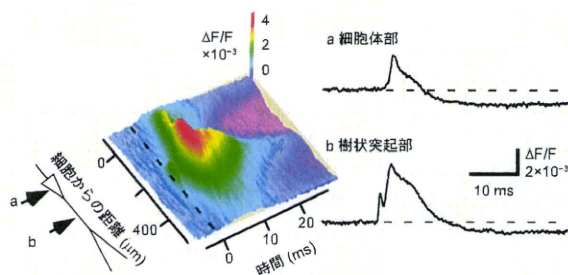
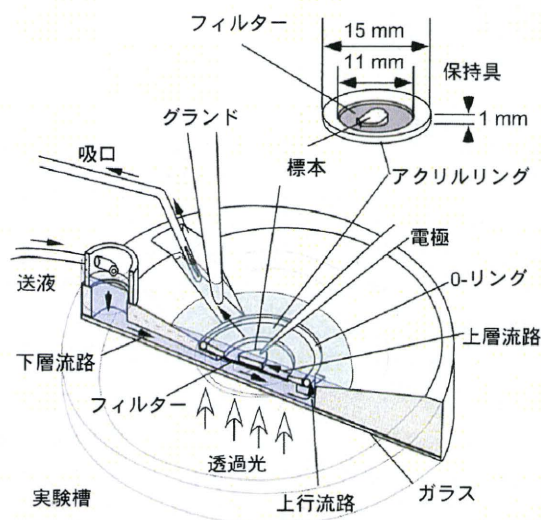


図2 海馬 CA1 野への電気刺激に対する膜電位応答を膜電位感受性色素によって計測したときの典型的な光信号 [ $\Delta F/F$ :初期蛍光強度 (F) に対する蛍光強度の変化量 ( $\Delta F$ ) 比]。細胞に沿った電位変化分布の時間変化 (左) と代表ピクセル (a:細胞体部, b:樹状突起部) での信号 (右)。(電子ジャーナルではカラー)

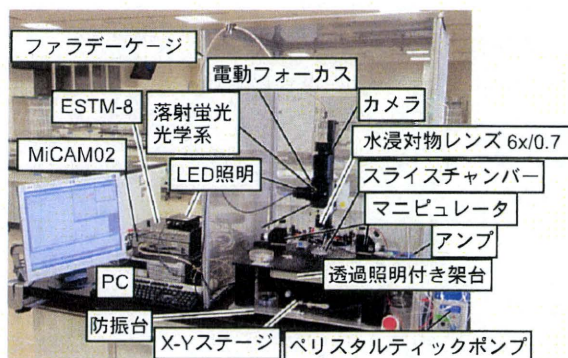


図3 チャンパーシステム図と実習システム写真。(電子ジャーナルではカラー)

学系を作製した。実体顕微鏡の対物レンズには開口数  
が大きなレンズがあったのでライカ社の実体顕微鏡用  
のレンズ (MZ-APO PLAN APO 1.0x) を投影レンズに  
使い、その間を無限遠焦点系とした落射蛍光光学系を  
作成した。実験槽中を還流している生理的塩溶液の水  
面がゆれると、機械的なノイズとして計測の邪魔にな  
る。対物レンズとしては、オリンパス光学に依頼して  
開発した低倍の高開口数の水浸対物レンズ (MYCAM  
10X/0.7, 5X/0.8) や、ブレインビジョン社の 6X/0.7  
の水浸レンズなども使用できる。

### 5.3 光計測撮像装置と刺激装置

上記の光学系と、光学計測装置、マニピュレータ  
2台をセット可能な光学定盤を使って、最小システム  
を組み上げた (図3)。5 mm 厚のステンレス板とソ  
ルボレインのダンパーで作成した防振台で十分な防振が  
得られる。これに、組み立て式のフェラデーケージを  
かぶせて、暗幕で遮光している。光源は補正付き  
LED を使用している。

光計測装置としてはブレインビジョン社の MiCAM-  
02 を採用し、電気刺激装置として ESTM-8 を採用し  
た。電気生理学的な活性をモニターしつつ、光計測を  
行っている。

全体の大きさは、底面積で 60 × 60 cm. 高さが 1 m  
である。これに PC が 1 台と電気生理用のアンプ (た  
とえば A-M Systems 社, Model 3100) とペリスタル  
ティックポンプがあれば実験が可能である。この大き  
さなら、通常の実験用機の一角でも複数台ならべて実  
験することができる。

### 5.4 ソフトウェア

実験の進行は IgorPro (Wavemetrics 社) にマクロを  
組んで自動化している。このソフトウェアで随時電極  
から記録される神経応答 (興奮性シナプス後電位、  
EPSP) を記録し、応答強度 (初期 EPSP スローブ) を  
リアルタイムでグラフにして表示している。このた  
め、実験者は実験の結果をリアルタイムに見ることが  
可能である。このときの電気刺激と、電気応答の波形  
記録には ESTM-8 を用いている。このソフトウェア  
は、要望があれば分けることができるので、必要な方  
は連絡してほしい。

## 6. おわりに

駆け足で、システムの紹介をしてきた。筆者は、こ  
のシステムで徳島文理大学薬学部の 3 年生を対象に  
学生実習を行っている。スライス研究室で教員が作  
成する。午前中に 10 枚程度スライスを作成し、実習

の開始時間に 3 階離れた実習室までスライスを運んで  
実験に供する。その後、電極の配置など目を配る必要  
はあるが、100 名ほどの学生さんが脳スライス標本か  
ら解析に必要なレベルの光信号を計測している様は  
10 年前には想像しにくかったことだ。光計測は、ふ  
だんは見えない神経信号を目に見える形に変えてくれ  
る。ディスプレイの上で動く膜電位変化の流れのよう  
すを見るだけでも脳の信号処理の一端がイメージでき  
る。これから長寿社会で神経関連の病気に社会をあげ  
て対応する必要がある今、これを体験した人材を供給  
することは意義深い。

また、このシステムは小型で扱いやすく電気生理な  
どの技術に熟練した計測者でなくとも複数の装置での  
同時データ取得が可能である。この利点を活かして、  
医薬品、食品成分、環境化学物質などの化学物質によ  
る神経影響評価への応用をめざした共同研究を、国立  
医薬品食品衛生研究所・毒性部の種村健太郎博士と進  
めている。

さて、ここまで簡単になって学部学生でもできるこ  
の夢の実験系、使ってみてはいかがでしょう？

この研究は平成 18 年、平成 20、21 年徳島文理大学  
「特色ある教育研究」ならびに厚生労働省科研費 (H20-  
化学一般-009) にサポートされた。

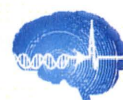
## 文 献

- 1) Tasaki, I. *et al.* (1968) Proc. Natl. Acad. Sci. USA 61, 883.
- 2) Salzberg, B. M. *et al.* (1973) Nature 246, 508.
- 3) 市川道教ら (1992) 日本物理学会誌 47, 707-712.
- 4) 飯島敏夫ら (1994) 生物物理 34, 219-222.
- 5) 松本 元 (1995) 生物物理 35, A25-A29.
- 6) Grinvald, A., Hildesheim, R. (2004) Nat. Rev. Neurosci. 5, 874.
- 7) Tominaga, T. *et al.* (2000) J. Neurosci. Methods 102, 11.
- 8) Tanemura, K. *et al.* (2002) J. Neurosci. 22, 133.
- 9) Kajiwara, R. *et al.* (2007) Eur. J. Neurosci. 25, 3648.
- 10) Tominaga, T., Tominaga, Y. (2010) Pflügers Arch. 460, 875-889.



富永貴志

富永貴志 (とみなが たかし)  
徳島文理大学香川薬学部准教授  
理化学研究所脳科学総合研究センター客員研究員  
理化学研究所脳科学総合研究センタースタッフサイ  
エンティストなどを経て現職。  
研究内容: 光計測を使った脳機能解析, 繊毛の分子  
機構解析  
連絡先: 〒769-2193 香川県さぬき市志度 1314-1  
E-mail: tominagat@kph.bunri-u.ac.jp  
富永洋子 (とみなが ようこ)  
徳島文理大学香川薬学部技術補佐員  
富士通, 理化学研究所脳科学総合研究センターテ  
クニカルスタッフなどを経て現職。  
研究内容: 光計測を使った脳機能解析



RESEARCH

Open Access

# The physiological roles of vesicular GABA transporter during embryonic development: a study using knockout mice

Kenzi Saito<sup>1,2</sup>, Toshikazu Kakizaki<sup>1,3</sup>, Ryotaro Hayashi<sup>4</sup>, Hiroshi Nishimaru<sup>5</sup>, Tomonori Furukawa<sup>6</sup>, Yoichi Nakazato<sup>7</sup>, Shigeo Takamori<sup>8</sup>, Satoe Ebihara<sup>9</sup>, Masakazu Uematsu<sup>10</sup>, Masayoshi Mishina<sup>11</sup>, Jun-ichi Miyazaki<sup>12</sup>, Minesuke Yokoyama<sup>13</sup>, Shiro Konishi<sup>13</sup>, Koichi Inoue<sup>6</sup>, Atsuo Fukuda<sup>6</sup>, Manabu Fukumoto<sup>4</sup>, Kenji Nakamura<sup>13</sup>, Kunihiro Obata<sup>14</sup>, Yuchio Yanagawa<sup>1,3\*</sup>

## Abstract

**Background:** The vesicular GABA transporter (VGAT) loads GABA and glycine from the neuronal cytoplasm into synaptic vesicles. To address functional importance of VGAT during embryonic development, we generated global VGAT knockout mice and analyzed them.

**Results:** VGAT knockouts at embryonic day (E) 18.5 exhibited substantial increases in overall GABA and glycine, but not glutamate, contents in the forebrain. Electrophysiological recordings from E17.5-18.5 spinal cord motoneurons demonstrated that VGAT knockouts presented no spontaneous inhibitory postsynaptic currents mediated by GABA and glycine. Histological examination of E18.5 knockout fetuses revealed reductions in the trapezius muscle, hepatic congestion and little alveolar spaces in the lung, indicating that the development of skeletal muscle, liver and lung in these mice was severely affected.

**Conclusion:** VGAT is fundamental for the GABA- and/or glycine-mediated transmission that supports embryonic development. VGAT knockout mice will be useful for further investigating the roles of VGAT in normal physiology and pathophysiological processes.

## Background

GABAergic and glycinergic neurotransmissions play critical roles in the central nervous system (CNS), because they regulate network activity and are essential for a number of brain functions, such as cognition, perception, movement and respiration. In the adult mammalian CNS, GABA and glycine are the main inhibitory neurotransmitters, but in fetal life and early postnatal development, both neurotransmitters act as either excitatory or inhibitory, depending on the intracellular chloride concentration.

GABA is synthesized from glutamic acid by glutamate decarboxylase (GAD) [1] and is accumulated into synaptic vesicles by the vesicular GABA transporter

(VGAT) [2,3]. Two isozymes of GAD, GAD65 and GAD67, are primarily expressed in GABAergic neurons [4,5]. GAD65 knockout mice exhibit spontaneous seizures, elevated anxiety and altered sensitivity to pain [6,7]. GAD67 knockout mice die of cleft palate at birth [8]. VGAT is present in both GABAergic and glycinergic neurons and is also called the vesicular inhibitory amino acid transporter (VIAAT) [3,9]. In addition to its presence at GABAergic and glycinergic synapses, the role of VGAT/VIAAT in GABA and glycine release is supported by electrophysiological evidence from primary cultured hippocampal or spinal cord neurons of VGAT knockout mice [10] and VGAT-transfected secretory cells [11]. VGAT knockout mice die perinatally and show a hunched posture, cleft palate and omphalocele [10].

Divergent roles for the VGAT proteins are implicated in the nervous system. However, the contribution of

\* Correspondence: yanagawa@med.gunma-u.ac.jp

<sup>1</sup>Department of Genetic and Behavioral Neuroscience, Gunma University Graduate School of Medicine, Maebashi 371-8511, Japan  
Full list of author information is available at the end of the article



VGAT to tissues or cells outside of the CNS remains largely unclear. For example, neither muscle, lung nor liver phenotypes have been reported for these knockout mice. We independently generated VGAT knockout mice. To further investigate the roles of VGAT during development, we performed histopathological analyses in VGAT knockout muscle, lung and liver at an embryonic stage. These mice showed a reduction in the trapezius muscles, smaller saccules in the lung, and congestion in the liver. In addition, in VGAT knockout spinal cord motoneurons (MNs), spontaneous inhibitory postsynaptic currents (IPSCs) were absent. These experiments indicate that VGAT has an important role in the GABA- and/or glycine-mediated transmission that supports life. Preliminary results have been published in an abstract form [12].

## Results

### Generation of VGAT<sup>-/-</sup> mice

The targeting strategy used for the generation of VGAT knockout mice is shown in Figure 1A. Exons 2 and 3 encode the putative ten-transmembrane domain and C-terminus of the VGAT protein [3,13], and accordingly, the deletion of these regions was expected to destroy the function of the VGAT protein. Correctly targeted ES cell clones isolated were microinjected into blastocysts to generate chimeric mice. These mice were then crossed with C57BL/6 mice to generate heterozygous mice carrying one floxed allele (VGAT<sup>floxneo/+</sup> mice).

We generated the VGAT knockout allele by crossing VGAT<sup>floxneo/+</sup> mice with CAG-Cre mice, in which Cre recombinase is expressed ubiquitously [14]. Genotyping was performed by Southern blot analysis (Figure 1B) and PCR (Figure 1C), and the DNA sequences around the loxP site in the knockout allele were also confirmed (data not shown). To obtain homozygous VGAT knockout (VGAT<sup>-/-</sup>) mice, we intercrossed the VGAT<sup>+/-</sup> mice. Western blot analysis revealed no VGAT protein expression in embryonic day (E) 18.5 VGAT<sup>-/-</sup> brain, whereas VGAT protein expression in VGAT<sup>+/-</sup> mouse brains was reduced to about half of the wild-type level (Figure 1D). All E18.5 VGAT<sup>-/-</sup> fetuses displayed cleft palate (Figure 1E) and omphalocele (Figure 1F), phenotypes that are consistent with those described by Wojcik et al. [10].

No VGAT<sup>-/-</sup> mice survived beyond birth (Table 1). To estimate the time of death of VGAT<sup>-/-</sup> mice, we performed timed matings of the VGAT<sup>+/-</sup> mice and obtained the fetuses via cesarean section. Among the E18.5 offspring derived from the intercrosses of VGAT<sup>+/-</sup> mice, VGAT<sup>-/-</sup> fetuses were obtained at the expected Mendelian ratio (27.3%, 77 VGAT<sup>-/-</sup> of 282 littermates) and more than 97% of them (75 of 77) were alive (judged by their umbilical beats or heartbeats,

Table 1). When delivered by cesarean section on E18.5, both VGAT<sup>+/-</sup> (7 of 7) and VGAT<sup>+/-</sup> (11 of 12) fetuses began respiration, but none of the VGAT<sup>-/-</sup> fetuses (n = 7) began to breathe. Therefore, it is probable that VGAT<sup>-/-</sup> mice died at birth due to respiratory failure.

### Elevations in GABA and glycine contents in VGAT<sup>-/-</sup> forebrains

In the absence of vesicular storage, neurotransmitter levels can be altered, and this alteration depends on the absence of the vesicular transporter. For example, monoamines are drastically reduced in vesicular monoamine transporter 2 knockout brains [15], but acetylcholine (ACh) is increased in vesicular acetylcholine transporter (VAChT) knockout brains compared to control wild-type brains [16]. Therefore, we measured the amount of the neurotransmitters, GABA, glycine and glutamate in E18.5 VGAT<sup>-/-</sup> forebrain by HPLC. As shown in Figure 2A, VGAT<sup>-/-</sup> fetuses showed significant increases in both GABA and glycine, but not glutamate, compared to VGAT<sup>+/-</sup> fetuses. It is possible that the increase in GABA content in VGAT<sup>-/-</sup> fetuses was due to the elevated expression levels of GABA-synthesizing enzymes. To test for this possibility, we analyzed the expression levels of GAD65 and GAD67 in the embryonic brains. Our Western blot analysis showed that the expression levels of both GAD65 and GAD67 in VGAT<sup>+/-</sup> and VGAT<sup>-/-</sup> brains were similar (Figure 2B). These results indicate that the increase in GABA content was not derived from elevated amounts of GABA-synthesizing enzymes in VGAT<sup>-/-</sup> embryos.

### Absence of functional inhibitory synaptic transmission in the VGAT<sup>-/-</sup> spinal cord

To examine the physiological nature of synaptic inputs to spinal MNs, we performed whole-cell patch-clamp recordings using isolated spinal cord preparations taken from VGAT<sup>-/-</sup> and control mouse embryos. In these preparations, the neuronal connections within the spinal cord are kept relatively intact [17]. In control lumbar MNs, spontaneous outward currents were observed when the membrane potential was depolarized at -40 mV above the chloride ion reversal potential (approximately -78 mV in the present experimental condition). These currents were blocked by bath application of the glycinergic antagonist strychnine and the GABAergic antagonist picrotoxin, indicating that the currents were IPSCs (n = 8, Figure 3A). In contrast, we did not detect such spontaneous IPSCs in VGAT<sup>-/-</sup> MNs (n = 12, Figure 3B). When the membrane potential was held at -70 mV, spontaneous inward currents were observed both in control and VGAT<sup>-/-</sup> MNs (Figure 3A and 3B). These inward currents were abolished by the concomitant bath application of the ionotropic



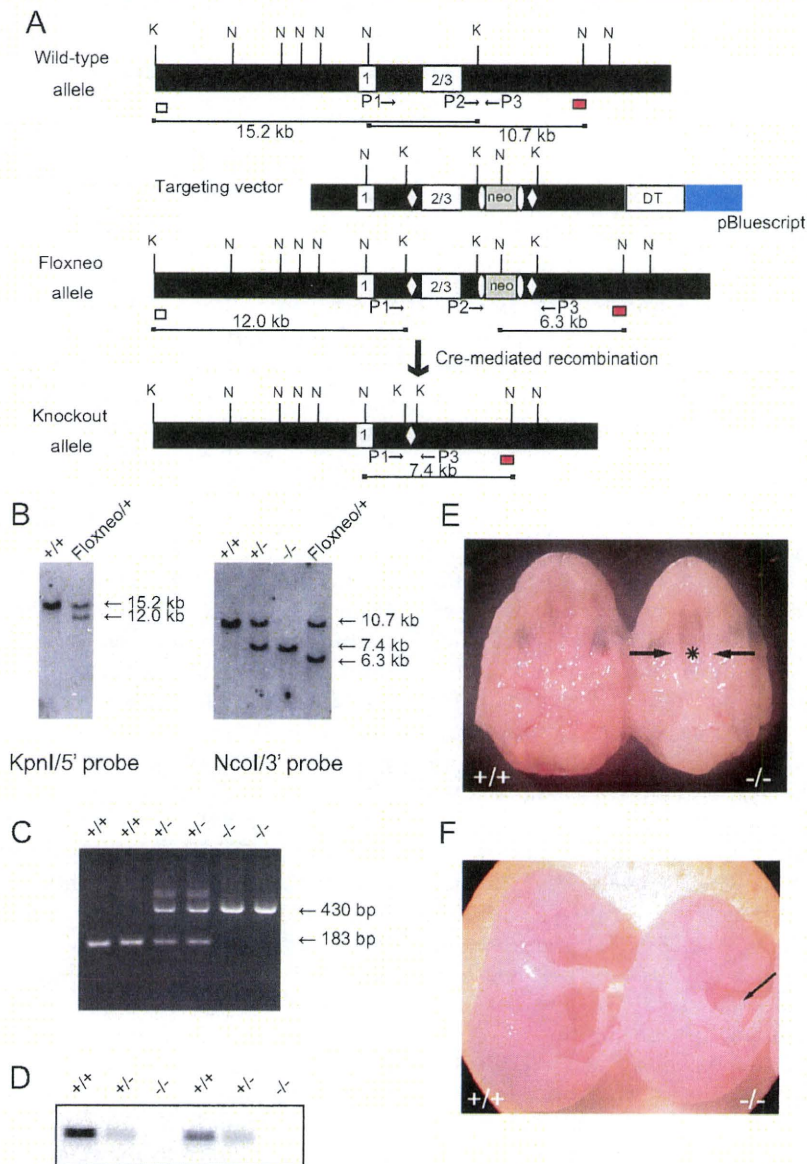


**Figure 1 Generation of  $VGAT^{-/-}$  mice.** (A) Schematic representation of the wild-type  $VGAT$  allele, the targeting vector, the  $VGAT$ -floxneo allele, and the  $VGAT$  knockout allele. Exons are represented by numbered white boxes. LoxP sites (open diamonds) and a PGK-Neo cassette (neo; gray box) flanked by the  $\text{frt}$  sites (open ellipses) were introduced into the wild-type  $VGAT$  locus by homologous recombination to produce the floxneo allele. The probes used for Southern blot analysis are indicated as white (5' probe) and red (3' probe) boxes. The expected sizes of the KpnI- and NcoI-digested genomic DNA fragments hybridized with the 5' and 3' probes, respectively, are indicated as lines under the schemes. Relevant restriction sites are indicated as follows: K, KpnI; N, NcoI. PCR primers are indicated as arrows. (B) (Left) Southern blot analysis of KpnI-digested genomic DNA isolated from  $VGAT^{+/+}$  (+/+) and  $VGAT^{floxneo/+}$  (Floxneo/+) mice using the 5' probe indicated in A. The wild-type allele corresponds to the 15.2 kb band, whereas the floxneo allele corresponds to the 12.0 kb band. (Right) Southern blot analysis of NcoI-digested genomic DNA isolated from  $VGAT^{+/+}$  (+/+) ,  $VGAT^{+/-}$  (+/-) ,  $VGAT^{-/-}$  (-/-) , and  $VGAT^{floxneo/+}$  (Floxneo/+) mice using the 3' probe indicated in A. The wild-type allele, the knockout allele, and the floxneo allele correspond to the 10.7 kb, 7.4 kb, and 6.3 kb bands, respectively. (C) Genotyping of offspring from intercrosses of  $VGAT^{+/-}$  mice by PCR. Three primers were used (see Methods). Primers P2 and P3 produce a 183 bp fragment that represents the wild-type allele, whereas primers P1 and P3 produce a 430 bp fragment that represents the knockout allele. (D) Western blot analysis of E18.5 whole brain homogenates from  $VGAT^{+/+}$  (+/+) ,  $VGAT^{+/-}$  (+/-) ,  $VGAT^{-/-}$  (-/-) using the anti-VGAT antibody directed against an N-terminal epitope. (E) Ventral views of the upper jaw of E18.5  $VGAT^{+/+}$  (+/+) and  $VGAT^{-/-}$  (-/-) mice. In contrast to the completely fused palate of a  $VGAT^{+/+}$  mouse, secondary palatal shelves of a  $VGAT^{-/-}$  mouse did not contact each other (arrows), and its nasal cavity (asterisk) could be seen. (F) Lateral views of E18.5  $VGAT^{+/+}$  (+/+) and  $VGAT^{-/-}$  (-/-) mice. An arrow indicates omphalocele in a  $VGAT^{-/-}$  mouse. In addition, the  $VGAT^{-/-}$  mouse showed an extremely hunched position in contrast to the  $VGAT^{+/+}$  mouse.

**Table 1 Genotypes of offspring from intercrosses of VGAT<sup>+/-</sup> mice and phenotypes of VGAT<sup>-/-</sup> mice**

Age	Genotype			Phenotype		
	+/+	+/-	-/-	No. of -/- found dead	No. of -/- with omphalocele	No. of -/- with cleft palate
E18.5	69 (24.5%)	136 (48.2%)	77 (27.3%)	2/77*	77/77*	29/29*
Newborn	22 (19.6%)	76 (67.9%)	14 (12.5%)	14/14*	Not determined	Not determined

\*affected/examined.

glutamate receptor blockers, a non-NMDA receptor antagonist 6-cyano-7-nitroquinoxaline-2,3-dione (CNQX) and an NMDA receptor antagonist D-2-amino-5-phosphonovaleric acid (AP5), indicating that MNs received excitatory synaptic transmission in the VGAT<sup>-/-</sup> spinal cord.

#### Alterations in body weight, response to stimuli, trapezius muscle, liver and lung of VGAT<sup>-/-</sup> mice

Wojcik et al. [10] reported that VGAT<sup>-/-</sup> mice display the phenotypes such as cleft palate, omphalocele, hunched posture, immobility and stiffness. However, we proposed that there would be some other alterations in VGAT<sup>-/-</sup> mice because VGAT is an essential molecule for GABAergic and glycinergic transmission. To address the question whether VGAT is essential for fetal growth, we initially measured the body weight of VGAT<sup>-/-</sup> fetuses compared to VGAT<sup>+/+</sup> and VGAT<sup>+/-</sup> littermates. The body weight of the E18.5 VGAT<sup>-/-</sup> fetuses was significantly lower than that of VGAT<sup>+/+</sup> and VGAT<sup>+/-</sup> fetuses (VGAT<sup>+/+</sup>: 1.18 ± 0.11 grams, n = 17; VGAT<sup>+/-</sup>: 1.20 ± 0.08 grams, n = 45; VGAT<sup>-/-</sup>: 1.05 ± 0.11 grams, n = 32 [mean ± SD], P < 0.001, one-way ANOVA, post hoc Fisher's least significant difference test). These results indicate that VGAT is important for fetal growth.

VGAT<sup>-/-</sup> fetuses exhibited immobility and lacked spontaneous limb and body movements, which are consistent with a report by Wojcik et al. [10]. To further address the question of whether the lack of movement in VGAT<sup>-/-</sup> fetuses was restricted to a defect in spontaneous movement, we examined the response of E18.5 VGAT<sup>-/-</sup> fetuses to mechanical stimuli. VGAT<sup>+/+</sup>, VGAT<sup>+/-</sup> and VGAT<sup>-/-</sup> fetuses were obtained via cesarean section and maintained alive in phosphate buffered saline. None of the VGAT<sup>-/-</sup> fetuses (n = 16) responded to a pinch of the tail by forceps, but all VGAT<sup>+/+</sup> (n = 16) and VGAT<sup>+/-</sup> (n = 53) fetuses responded with a twisting of the trunk. These results suggest that VGAT<sup>-/-</sup> fetuses suffer from severe impairments in motor function.

Because the hunched posture observed in VGAT<sup>-/-</sup> mice (Figure 1F) suggested defects in skeletal muscles or bones [18,19], we performed a histological examination of skeletal muscles and bones in the E18.5 embryos. Trapezius muscle was thinner in VGAT<sup>-/-</sup> mice than in the

control mice (Figure 4A, B). The VGAT<sup>-/-</sup> ribs in the lower part were depressed, and their position was retracted toward the inside compared to control (Figure 4C, D). Furthermore, the spaces between each rib appeared narrower in VGAT<sup>-/-</sup> mice compared to the control mice (Figure 4C, D). Abdominal organs were examined histologically in an attempt to identify pathological findings associated with defects in VGAT<sup>-/-</sup> mice. Not only omphalocele (Figure 1F) but also hepatic congestion were characteristic of VGAT<sup>-/-</sup> embryos (Figure 4E, F). These results suggest that the crouching posture caused by an imbalance of the strength between the dorsal and ventral muscles made the thorax expand ineffectively, leading to an increase in intra-abdominal pressure in VGAT<sup>-/-</sup> embryos. Although omphalocele can be caused by a malformation of the ventral body wall [20], the rectus abdominis muscle showed no apparent abnormality in VGAT<sup>-/-</sup> mice (data not shown).

The VGAT<sup>-/-</sup> mice lacked autonomous and joggling-induced breathing movements, consistent with the report by Fujii et al. [21]. However, there is still uncertainty regarding the mechanism responsible for the respiratory failure caused by the loss of VGAT protein. To understand the pathology causing respiratory failure in VGAT<sup>-/-</sup> mice, we fixed embryos at E18.5, the day prior to birth, and performed pathohistology of the lungs. Examination under a microscope revealed that the VGAT<sup>-/-</sup> lung barely contained alveolar spaces compared to the control lung (Figure 4G, H). A possible cause of atelectasis was reported defect in the diaphragm [22]. We examined the VGAT<sup>-/-</sup> diaphragm histologically, but we didn't detect any difference in the diaphragm between the VGAT<sup>-/-</sup> and control mice.

The alterations in the VGAT<sup>-/-</sup> muscle, liver and lung were likely caused by the loss of VGAT in the CNS, but not the loss of VGAT in the peripheral tissue because VGAT transcripts were detected in brain and spinal cord, but not in muscle, liver or lung [2,3].

#### Comparison of cleft palate and omphalocele between VGAT<sup>-/-</sup> mice and GAD67<sup>-/-</sup> mice

Cleft palate is exhibited by VGAT<sup>-/-</sup> and GAD67<sup>-/-</sup> mice [8,10,23], demonstrating that GABAergic transmissions are involved in palatogenesis. Because VGAT and

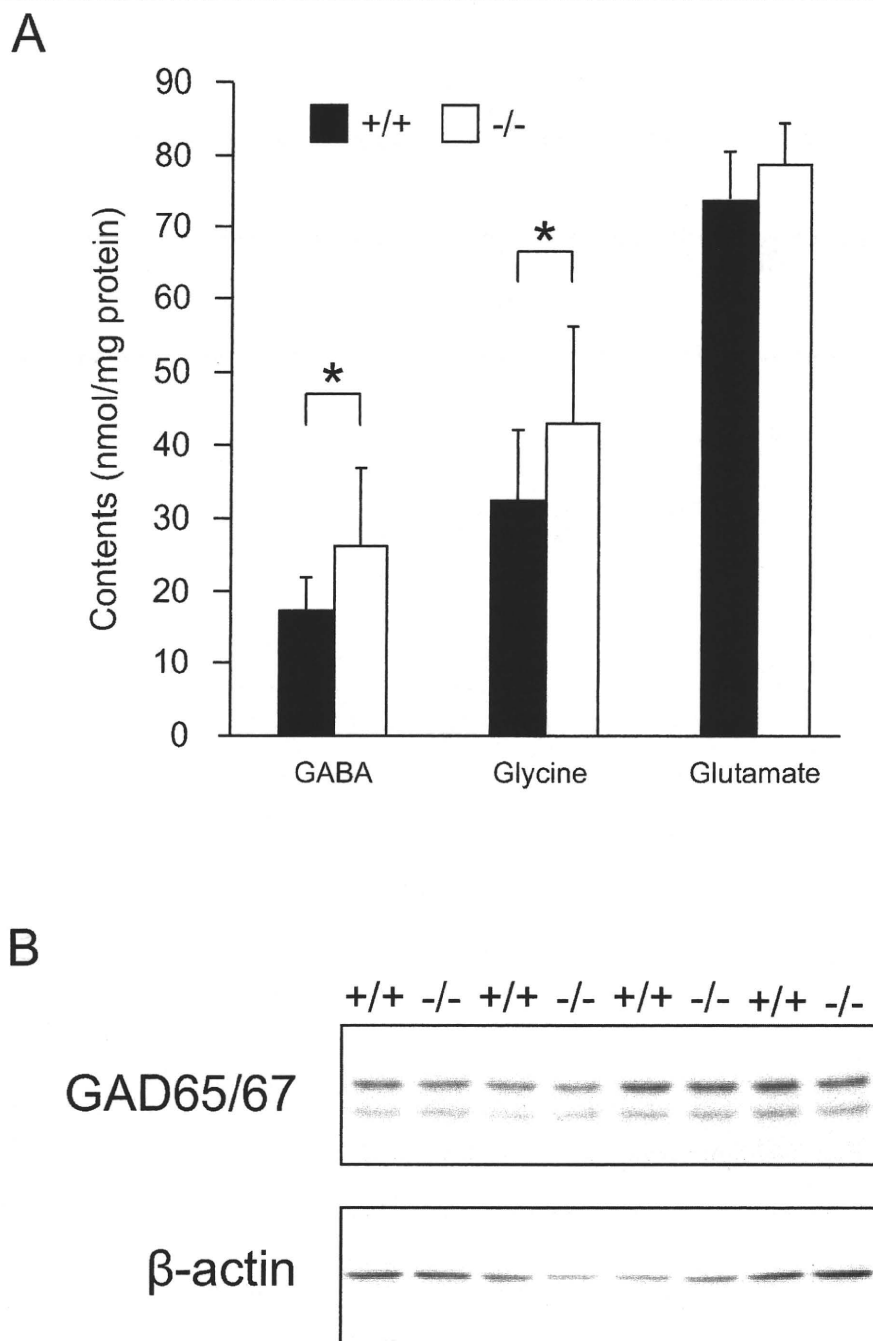
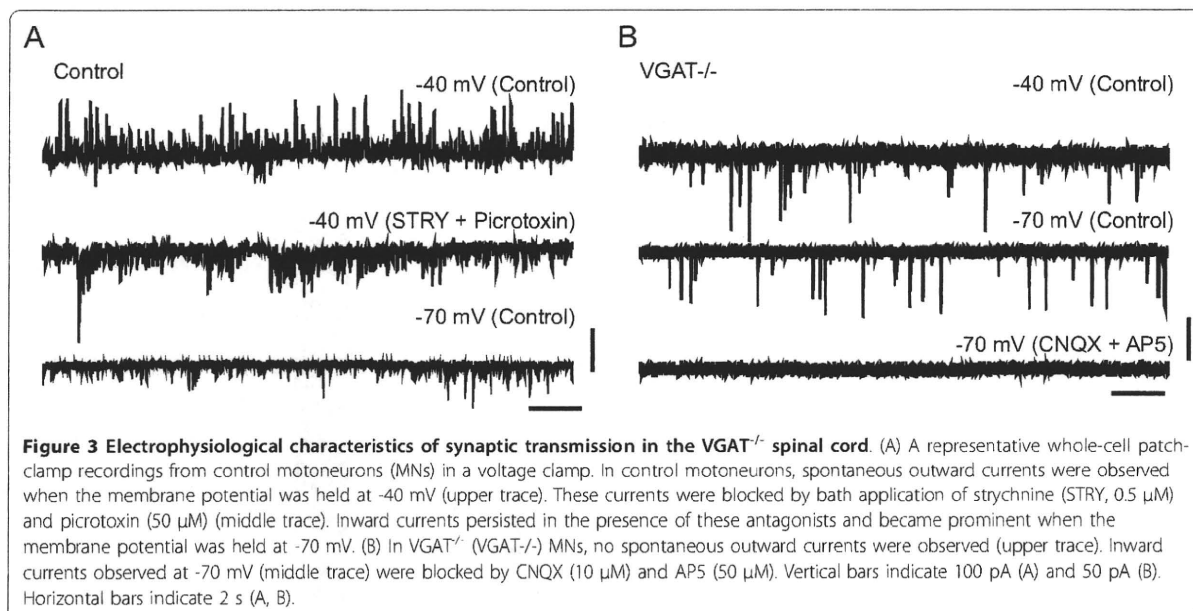


**Figure 2 Neurotransmitter contents and expression levels of GAD65 and GAD67.** (A) Neurotransmitter contents of E18.5 mouse forebrain. VGAT<sup>-/-</sup> mice showed significantly higher levels of GABA and glycine than VGAT<sup>+/+</sup> mice, but not glutamate. Values represent means  $\pm$  SD (\* $P < 0.05$ ; Student's t-test,  $n = 5-13$  per group). (B) Western blot analysis. The expression level of GAD65 and GAD67 in whole brain homogenates was not significantly different between VGAT<sup>+/+</sup> (+/+) and VGAT<sup>-/-</sup> (-/-) mice. Equal amounts of protein were loaded and probed with an antibody that recognizes both GAD65 and GAD67. For the statistical comparison, the same blot was probed with anti- $\beta$ -actin antibody as an internal control and measurements for GAD65 and GAD67 bands were normalized to the  $\beta$ -actin bands (GAD65: VGAT<sup>+/+</sup>  $100 \pm 23\%$ ; VGAT<sup>-/-</sup>  $111 \pm 20\%$ ,  $n = 4$ ,  $P = 0.71$ ) (GAD67: VGAT<sup>+/+</sup>  $100 \pm 18\%$ ; VGAT<sup>-/-</sup>  $93 \pm 17\%$ ,  $n = 4$ ,  $P = 0.80$ ).



GAD67 exhibit different molecular functions, we investigated whether the severity of cleft palate was different between VGAT<sup>-/-</sup> and GAD67<sup>-/-</sup> mice. Figure 5A shows hematoxylin-eosin staining of coronal sections from the oral region. In the cleft palate of VGAT<sup>-/-</sup> mice, the palatal shelves remained vertical along the sides of the tongue (3 of 3). However, in GAD67<sup>-/-</sup> mice, the palatal shelves were elevated up to a horizontal position (3 of 3). In one of the GAD67<sup>-/-</sup> mice, the palatal shelves even fused with each other completely (data not shown). These observations suggest that palatogenesis progresses further in GAD67<sup>-/-</sup> mice than in VGAT<sup>-/-</sup> mice. Our observations also suggest that cleft palate in VGAT<sup>-/-</sup> mice is more severe than in GAD67<sup>-/-</sup> mice.

The observation of omphalocele in VGAT<sup>-/-</sup> mice prompted us to investigate whether GAD67<sup>-/-</sup> mice displayed omphalocele. We found omphalocele in GAD67<sup>-/-</sup> and VGAT<sup>-/-</sup> mice (Figure 5B), indicating that GABA signaling is involved in its onset. The incidence rate of omphalocele in GAD67<sup>-/-</sup> mice was 43% (17 of 40), whereas the incidence in VGAT<sup>-/-</sup> mice was 100% (77 of 77; see also Table 1). Thus, the penetrance of omphalocele in GAD67<sup>-/-</sup> mice was lower than in VGAT<sup>-/-</sup> mice. The size of omphalocele appeared to be larger in VGAT<sup>-/-</sup> mice than in GAD67<sup>-/-</sup> mice. Taken together, these data suggest omphalocele in GAD67<sup>-/-</sup> mice is less severe than in VGAT<sup>-/-</sup> mice, similar to what was observed with the cleft palate.

## Discussion

The present work addresses the contribution of VGAT to embryonic development. We generated VGAT mice

and found that VGAT is fundamental for GABA and/or glycine release in the spinal cord. Moreover, in the absence of VGAT, there are profound effects on muscle, liver and lung during embryonic development. These observations bear important consequences for understanding the functional roles of VGAT from the cellular to the whole-body level.

## Generation of VGAT knockout mice

Wojcik et al. [10] generated VGAT knockout mice, in which a mutation was inserted into exon 1, and these mice exhibit cleft palate and omphalocele. Here, we generated floxed VGAT knockout mice, in which exons 2 and 3 of the VGAT gene were flanked by loxP sites. Crossing the floxed VGAT mice to CAG-Cre mice reproduced the phenotypes of cleft palate and omphalocele. Exons 1 and 2/3 encode the cytoplasmic domain and the transmembrane domain, respectively [3,13]. Our results demonstrate that exons 2 and 3 are dispensable for the function of VGAT.

VGAT<sup>floxneo/floxneo</sup> mice were born at the expected frequency, were viable, did not have a cleft palate or omphalocele, and were overtly indistinguishable from their wild-type littermates. Western blot showed that the level of VGAT protein expression in VGAT<sup>floxneo/floxneo</sup> brain was not different from the wild-type brain (Additional file 1: Supplementary Figure S1). These results suggest that a loxP sequence and an *frt*-flanked phosphoglycerate kinase promoter-driven neomycin-resistance gene (PGK-Neo) inserted into intron 1 and the 3'-flanking region of the VGAT gene, respectively, do not affect the expression level of VGAT protein. Therefore, the VGAT-floxneo